ASCE

Effect of Protein Containing Hydrogels on the Self-Healing of Cementitious Materials

Elvis Baffoe, S.M.ASCE[1]; and Ali Ghahremaninezhad[2]

Abstract: This study examined the effect of hydrogels containing urease and proteins on the self-healing of cracked cementitious materials. The encapsulation of proteins and urease decreased the absorption of hydrogels. It was shown that proteins were able to release from hydrogels into the surrounding cementitious matrix. TGA, FTIR, and SEM showed increased calcium carbonate formation, and optical imaging indicated enhanced crack filling in the samples with hydrogels containing urease and proteins, compared to the control sample. This is attributed to the enhanced autogenous healing provided by water absorption/desorption of hydrogels as well as enzymatic reaction. Calcite was shown to be the dominant polymorph of calcium carbonate in the healing products. Interestingly, the mechanical strength regain was markedly higher in the samples with hydrogels containing urease and proteins compared to the control sample. Improved interfacial strength at the microstructure level enhances cohesion within healing products and adhesion between the healing products and crack surface, leading to overall increased mechanical strength regain. The electrical resistivity results were shown to be in agreement with the mechanical strength regain. **DOI: 10.1061/JMCEE7.MTENG-17025.**

Introduction

Concrete is the most used construction material globally due to its low cost and high compressive strength (Tang et al. 2015). The increased demand for concrete has led to an increase in cement production worldwide. It is reported that cement production is responsible for 5%–8% of the anthropogenic carbon dioxide emissions (Prabahar et al. 2021). During the life span of concrete, it is subjected to different mechanical and environmental conditions that lead to the formation of cracks (Chindasiriphan et al. 2020). These mechanical and environmental conditions can take the form of shrinkage, freeze–thaw, excessive loading, etc. (Chindasiriphan et al. 2020). The formation and growth of cracks expose the concrete to various chemical and biological substances as they act as pathways for deleterious substances to infiltrate the concrete leading to the loss of durability and structural integrity. Globally, the repair or maintenance of concrete infrastructure is expensive, and the cost is expected to remain high (Chindasiriphan et al. 2020). The American Road & Transportation Builders Association (ARTBA) in their 2022 Bridge Report estimates that the cost of identified repairs for all 224,000 bridges, including the 43,578 structurally deficient, is $260 billion (Black 2022), suggesting that the cost of infrastructure repair is significant and poses a great burden on the national budget. The manual repair of cracks is expensive and labor-intensive (Huang et al. 2016; Snoeck et al. 2020). In addition, because most of the crack repairs are performed on the surface, deep or invisible cracks are not detected or repaired, and hence the structure is not able to fully recover its lost integrity (Snoeck et al. 2020). Concrete has the inherent mechanisms that allow it to heal itself in a process called autogenous healing (Snoeck et al. 2014b). Autogenous healing is a self-healing concept, where cracks are healed due to the ongoing hydration of the unhydrated cement or carbonation of calcium hydroxide (CH). In a study conducted by Schlangen et al. (2006), it was discovered that calcium–silicate–hydrate (C-S-H) was formed in the cracks after the cracked concrete was healed in water. The drawback of the autogenous healing is that it is limited to healing smaller cracks and hence not effective in healing larger cracks (Aldea et al. 2000; Reinhardt and Jooss 2003). It has been reported by Aldea et al. (2000) and Edvardsen (1999) that the maximum crack width that can be healed through the autogenous healing concept is within the range of 200 to 300 μm. In some studies, it was reported that the maximum width that could be healed was 100 μm, an indication that the autogenous healing concept in practice is not acceptable (Xu and Yao 2014).

To overcome this issue, a more efficient approach referred to as the autonomous self-healing concept has been investigated in recent years (Jonkers et al. 2008, 2010; Snoeck et al. 2014a; Wang et al. 2014b; Xu and Yao 2014; Zhu et al. 2020). In the autonomous healing concept, some chemical or biological agents are added to the concrete mixture. When cracks are formed, these agents are triggered to release the healing materials, which then react with some nutrients, oxygen, or moisture to initiate self-healing. Reports have shown that the autonomous healing concept is effective in healing cracks with larger widths (Tang et al. 2015).

Calcium carbonate ($CaCO_3$) precipitation via bacterial and enzymatic activities has gained attention as an autonomous crack-healing technique in recent years due to its environmental and health safety compared to the chemically based admixtures (Baffoe and Ghahremaninezhad 2022a; Dakhane et al. 2018; Xu and Yao 2014). One of the early studies on crack healing in cementitious materials using bacteria-induced calcium carbonate precipitation was reported by Gollapudi et al. (1995). Consequently, other researchers including Jonkers and Schlangen (2007) continued with the investigation. The study by Jonkers and Schlangen examined the potential application of calcite-precipitating bacteria as a crack-healing agent in concrete. It was reported in the study that

[1]Doctoral Student, Dept. of Civil and Architectural Engineering, Univ. of Miami, Coral Gables, FL 33146. Email: exb829@miami.edu

[2]Associate Professor, Chair of the Experimental Analysis and Instrumentation Committee, Dept. of Civil and Architectural Engineering, Univ. of Miami, Coral Gables, FL 33146 (corresponding author). ORCID: https://orcid.org/0000-0001-9269-801X. Email: a.ghahremani@miami.edu

Note. This manuscript was submitted on May 25, 2023; approved on November 3, 2023; published online on February 26, 2024. Discussion period open until July 26, 2024; separate discussions must be submitted for individual papers. This paper is part of the ***Journal of Materials in Civil Engineering***, © ASCE, ISSN 0899-1561.

the alkali-resistant spore-forming bacteria can precipitate calcite to heal freshly formed cracks in concrete (Gollapudi et al. 1995). Xu and Yao (2014) investigated the self-healing of cementitious materials using a nonureolytic bacteria-based healing agent and reported a full healing for up to 400 μm crack width. Dakhane et al. (2018) utilized enzyme-induced calcium carbonate precipitation (EICP) to repair cracked mortar prisms and reported a 33% flexural strength increase in the cracked mortar. Baffoe and Ghahremaninezhad (2022a) also investigated the crack surface binding of EICP using ground hardened cement paste as the crack surface model. They observed an improved tensile strength and porosity reduction of the samples treated with EICP.

The idea of self-healing is mimicked from the event of biological restoration, and bone-mimic materials that are developed by simulating the structure or composition of bones to develop self-healing performance in concrete (Li et al. 2018). The bone tissue structure is composed of an inorganic phase, primarily calcium phosphate, and a collagen protein, which makes the biological composite strong to resist deformation. Another example is abalone nacre, which is composed of about 95% brittle aragonite and 5% biomolecules and has a fracture toughness significantly higher than pure aragonite (Espinosa et al. 2011). This enhanced property is attributed to the role of certain biomolecules affecting the material behavior across multiple length scales (Baffoe and Ghahremaninezhad 2022a).

Proteins consist of a large number of amino acids with varied functional groups (Baffoe and Ghahremaninezhad 2022a, b). These functional groups include charged, hydrogen bond-forming, and hydrophobic groups (Baffoe and Ghahremaninezhad 2022a, b). The diversity of different functional groups in the molecular structure of proteins allows multiple pathways for the proteins to interact with inorganic phases and influence the growth, microstructure, and macroscale properties of materials resulting from biomineralization. Several groups have examined the effect of proteins on $CaCO_3$ mineralization and the morphological and polymorphic changes in $CaCO_3$ (Briegel et al. 2012; Li et al. 2018; Rodriguez-Navarro et al. 2007). Rodriguez-Navarro investigated the precipitation of $CaCO_3$ by extracellular polymeric substances and attributed the stabilization of vaterite to the presence of proteins (Rodriguez-Navarro et al. 2007). Sondi and Matijević (2001) observed proteins in vaterites precipitated by urease enzyme. Prior studies have indicated that certain biomolecules can bond to solid surfaces and enhance the cohesive and adhesive bonds in sediments and mineral precipitates (Costa et al. 2018; Martin et al. 2021; Tourney and Ngwenya 2014; Vignaga et al. 2012; Wu et al. 2014). The interaction between proteins and cementitious materials and their effect on surface binding have recently been investigated by Baffoe and Ghahremaninezhad (2022a, b). The contribution of protein to soil consolidation has also been evaluated by Almajed et al. (2019), where they observed a higher strength for EICP consolidated soils modified with nonfat milk dairy powder (NFMP).

The use of superabsorbent polymer (SAP), which is a type of polymeric hydrogels, as a means to develop self-healing cementitious materials has been at the center of investigation in recent years (Chindasiriphan et al. 2020; Mignon et al. 2015; Snoeck et al. 2020). When SAP is mixed with cementitious materials, it can absorb the liquid and swell to block the crack. It can also improve the autogenous self-healing by accelerating the hydration of unreacted phases and promoting the carbonation of CH (Snoeck et al. 2020). It has also been suggested that encapsulating microbial organisms into SAP can protect the microbial organisms from the aggressive cementitious environment (Wang et al. 2014a).

The effect of proteins on the formation and microstructure of the healing products and mechanical regain in cracked cementitious materials is not adequately understood. To address this research gap, in this study different proteins and urease were encapsulated in hydrogels, and their self-healing effect was investigated. We hypothesize that the use of hydrogels as an encapsulating medium can protect proteins and other agents against harsh environments at the early age of cementitious materials and provide water as a critical ingredient for the self-healing processes. We also hypothesize that the proteins are able to bind together the solid constituents of the healing products and also bind the healing products to the surfaces of the cracks, thereby improving the overall strength. The release behavior of the hydrogels in a cementitious matrix was examined. The mineralogical properties of the healing products were studied using thermogravimetric analysis (TGA), Fourier transform infrared spectroscopy (FTIR), scanning electron microscopy (SEM), and energy dispersive x-ray spectroscopy (EDX). The crack filling ability after a series of healing cycles was investigated using optical imaging. The strength regain of the healed samples was evaluated using compressive and flexural strength tests. The influence of crack healing on electrical resistivity as a measure of the transport property of the cement paste was also investigated.

Experiments

Materials

Cement Paste

A type I/II ordinary portland cement (OPC) was used in the preparation of cementitious samples. The chemical composition of the type I/II OPC is shown in Table 1.

Proteins

Three proteins with different molecular structures, namely, collagen peptide (CP), whey protein, and NFMP, were used in this study. The molecular structure and physicochemical properties of these proteins are well documented in previous studies (Arriaga 2011; Baffoe and Ghahremaninezhad 2022a, b; Masoule et al. 2023; Shoulders and Raines 2009; Singh 2007). Collagen peptide is a fibrous protein with high amount of hydroxyproline and proline (Raydan et al. 2021). NFMP is globular and comprises about 80% casein proteins (Bian 2012). Whey protein concentrate is a by-product of the cheese-making process and comprises four main classes of proteins, namely β-lactoglobulin, α-lactalbumin, serum albumin, and several immunoglobulins (Arriaga 2011). The availability of these proteins at the scale needed for the experiments conducted in this study as well as the variation in the characteristics of these proteins, including their functional groups and charged, hydrogen bond-forming, and hydrophobic groups, were factors for their selection in this study.

Table 1. Oxide composition of the type I/II ordinary portland cement used in this study

Oxide	Percentage (%)
CaO	64
SiO_2	20.6
Al_2O_3	4.8
Fe_2O_3	3.5
MgO	0.9
Na_2O	0.3
K_2O	0.1
SO_3	3.4
LOI	2.4
Total	100

Table 2. Composition of the hydrogels synthesized in the experiments

Hydrogel	DI water (g)	AM (g)	MBA (g)	APS (g)	Urease (kU/L)	Protein (%) by mass of DI water
H	200	40	0.1	1.28	—	—
H U	200	40	0.1	1.28	24	—
H U-whey protein	200	40	0.1	1.28	24	3
H U-CP	200	40	0.1	1.28	24	3
H U-NFMP	200	40	0.1	1.28	24	3

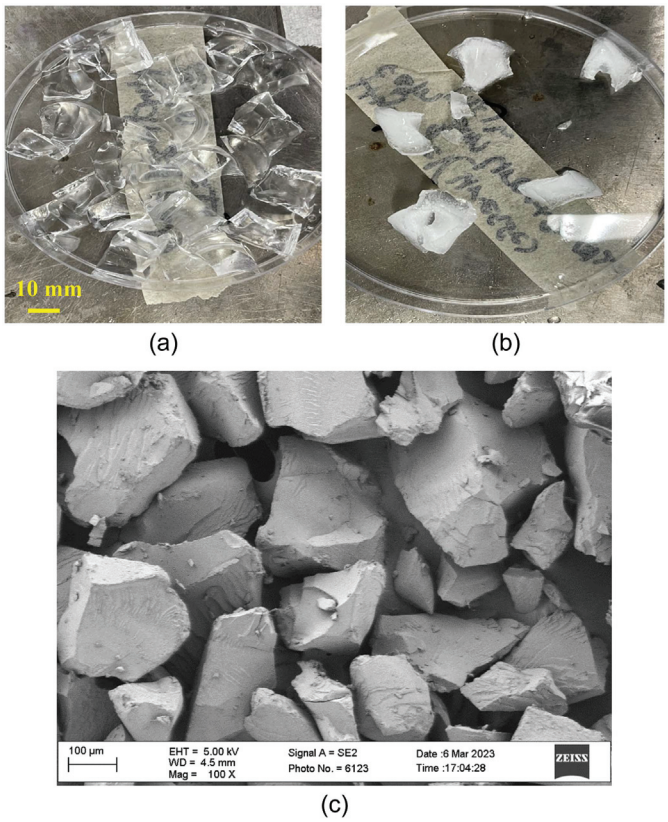

Fig. 1. (a and b) Optical image of H and H U, respectively, in the bulk form before drying and grinding; and (c) SEM image of H particles used in this study.

Hydrogels

The hydrogel utilized in the present study was crosslinked polyacrylamide that was synthesized using free radical polymerization (Farzanian et al. 2019, 2021; Vafaei et al. 2021). Polyacrylamide-based hydrogels are nontoxic and biocompatible and do not react with proteins or enzymes. They have been used in previous studies for encapsulating proteins in ion sensing and biomedical applications (Rrustemi et al. 2020; Tantimongcolwat et al. 2014; Ur Rehman et al. 2020). The chemical composition and designation of hydrogels prepared in this study are shown in Table 2. Chemicals for hydrogel preparation and urease were purchased from Sigma-Aldrich. In the preparation of hydrogels, 40 g of acrylamide monomers were added to 200 mL DI water containing 1 mL of urease with a concentration of 24 kU/L. The protein at a concentration of 3% by mass of acrylamide-urease solution was added and stirred for 5 min to allow the proteins to dissolve completely. Afterwards, 0.1 g of the crosslinker NN′-methylenebisacrylamide (MBA) was added to the solution. The solution was degassed for 5 min using argon gas, and then 1.28 g of ammonium persulfate (APS) as the initiator was added to the solution and stirred for an additional 10 min. Then, the solution was poured into a beaker, covered, and placed in an oven at 55°C to allow the solution to gel. After 3 h, the gelled solution was oven-dried at 50°C for 7 days. Dried hydrogels were ground into fine powder and sieved to obtain hydrogel powder within the size ranges of 75–425 μm and 425–1,000 μm. Hydrogel powders were double bagged and placed inside a desiccator until their use. Figs. 1(a and b) show the optical image of hydrogel H and the hydrogel containing urease H U, respectively, in the bulk form before being dried in an oven. While H appeared to be translucent, H U was opaque. Fig. 1(c) shows a SEM micrograph of H after being dried, ground, and sieved. The hydrogel particles show an angular morphology and various sizes.

Mix Design

Table 3 lists the mix proportions of the cement pastes used in this study. Plain cement paste without hydrogel served as the control, while the remaining mixes contained hydrogel (H), hydrogel-urease H U, or hydrogel-urease/protein. The mixes containing proteins were designated as H U-whey protein, H U-CP, and H U-NFMP. Oven-dried hydrogel powder was dry mixed with cement powder for 5 min using a mixer at a speed of 440 RPM. Bio-nutrients including urea and calcium nitrate $Ca(NO_3)_2 \cdot 4H_2O$ were dissolved in DI water for 3 min and slowly added to the cement powder and hydrogel mix. Mixing proceeded for 4 min until a uniform mix was obtained. For the compressive strength, compressive strength regain, and electrical resistivity tests, hydrogel particles with a size range of 75–425 μm were mixed with the cement paste. Meanwhile, for flexural strength regain, paste samples were mixed with hydrogels with a size range of 425–1,000 μm.

The fresh paste was cast into cube molds (50 mm × 50 mm × 50 mm) to study the compressive strength and electrical resistivity of the paste. For cube samples, hydrogel particles with the size range of 75–425 μm were used. The paste for flexural strength was cast into prisms of dimension 150 mm × 25 mm × 25 mm. The prismatic mold was filled to one-third of its height with plain cement paste of w/c = 0.4. The molds were placed on a vibration table for compaction. Following the protocol by Fahimizadeh et al. (2020), a layer of glass fiber was placed on the surface of the plain cement paste, and the remaining top two thirds of the mold was filled with cement pastes as listed in Table 3 and tamped for 1 min. The hydrogel particles used in the prisms were in the range of 425–1,000 μm. A schematic of a prism is shown in Fig. 2. The reason for placing a layer of glass fiber is to ensure the same crack width and length in all prisms. Both the cube and prism samples were covered with a polyethene sheet and placed in a plastic box in the laboratory. The samples were demolded after 24 h and cured in sealed double plastic bags for 21 days. The samples were then cracked and healed as discussed in the section "Mechanical Properties."

Table 3. Mix designs used in the experiment

Mix designation	W/C	% hydrogel by mass of cement	Urea (M)	$Ca(NO_3)_2 \cdot 4H_2O$ (M)
Control	0.5	—	1.5	1
H	0.5	3	1.5	1
H U	0.5	3	1.5	1
H U-whey protein	0.5	3	1.5	1
H U-CP	0.5	3	1.5	1
H U-NFMP	0.5	3	1.5	1

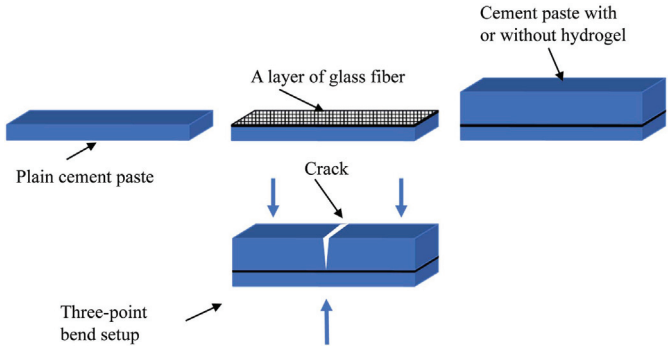

Fig. 2. Schematic of a paste prism for the flexural strength test.

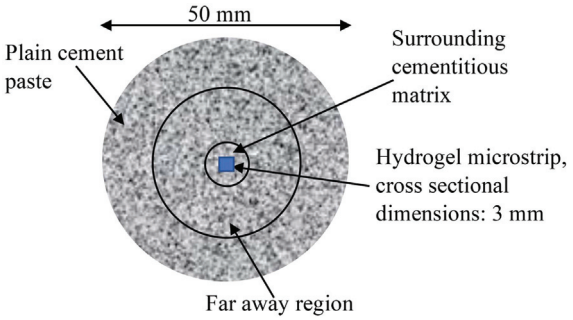

Fig. 3. Schematic showing the hydrogel microstrip embedded in cement paste.

Methods

Hydrogel Absorption

The absorption capacity of hydrogels or hydrogels containing urease/protein was evaluated using the teabag test (Farzanian et al. 2019, 2021; Vafaei et al. 2021; Wang et al. 2014a). The teabag test was performed in 0.5 M $CaCl_2$ solution and extracted cement pore solution. The extracted cement pore solution was prepared by mixing 10 g of cement powder with 100 mL of DI water and stirring continuously for 30 min. The cement mix was poured into centrifuge tubes and centrifuged at 4500 RPM for 5 min to remove undissolved particles. Urea at the concentration of 1.5 M was added to both 0.5 M $CaCl_2$ solution and cement pore solution and stirred for an additional 5 min. The initial weight of the teabag containing 0.1 g of dry hydrogel powder was determined. The teabag was submerged in the solution, and the solution was covered with a plastic membrane to minimize exposure to air. At different time intervals, the teabag was removed from the solution, surface dried on a paper towel, and its mass measured using a scale with a resolution of 0.001 g. The absorption was obtained using Eq. (1) below:

$$Q = \left(M_w\text{-}M_{wt}\text{-}M_s\right)/M_s \tag{1}$$

where M_w, M_{wt}, and M_s = masses of the wet teabag, wet teabag without hydrogel, and dry hydrogel, respectively. Three replicates were used for each hydrogel, and the average is reported.

Release of Proteins into Cementitious Matrix

The ability of the proteins to release from the hydrogels into the surrounding cementitious matrix and their survivability were investigated in this test. Hydrogels used in this test were synthesized using the same procedure described in the Section 2.1.3, except that hydrogels contained only proteins and they were prepared in thin layers as discussed in detail in previous papers (Farzanian and Ghahremaninezhad 2018a, c). Hydrogel microstrips were cut from hydrogel layers and dried in an oven at the temperature of 60°C for 3 days. The dry cross-sectional dimensions of the microstrip were about 3 mm. The hydrogel microstrips were placed in the axial direction at the center of a polypropylene tube (50 mm in diameter and 300 mm in length) containing cement paste with a $w/c = 0.4$. Fig. 3 depicts the schematic of the hydrogel microstrip embedded in a cementitious matrix. The sample was removed from the tube after 3 days of curing and broken in the longitudinal direction to gain access to the hydrogel microstrip and the cementitious matrix adjacent to the hydrogel microstrip. The cementitious matrix adjacent to the hydrogel microstrip was scraped and characterized using the Agilent 8453 UV-Vis spectrophotometer and bicinchoninic acid (BCA) to determine the presence and amount of proteins released from the microstrip into the cementitious matrix. The scraped cementitious matrix was mixed with 2 mL of BCA reagent and incubated in an oven for 30 min at 37°C. After 30 min of incubation, the mixture was cooled for 10 min at room temperature, centrifuged, and poured into cuvette. The absorbance values of the solution were recorded using the UV-Vis spectrophotometer. A purple color reveals the presence of protein in the solution (Smith et al. 1985). The standard (original) protein concentrations of individual proteins were also obtained and plotted against their respective absorbance values and a linear equation generated. By using the absorbance value of the proteins in the cementitious matrix, the concentration of the proteins in the cementitious matrix was determined. Another batch of samples scraped from the cementitious matrix adjacent to the hydrogel microstrip and far away (bulk paste) were used in the TGA and FTIR tests. The details of the TGA and FTIR tests are provided later in the paper.

Artificial Planar Crack Preparation

Artificial planar gaps of cement pastes with and without hydrogels were prepared to simulate cracks in cement paste. This allowed us to obtain enough healing products needed for chemical characterization. The mixing protocol and curing conditions of the samples for the artificial planar cracks were similar to the sample preparations described in the Section 2.1.4 and illustrated in Fig. 4. The hydrogel sizes used were in the range of 425 to 1,000 μm. After 21 days of curing, the samples were cut into slices of dimensions 15 mm × 50 mm × 50 mm and polished with SiC sandpapers with grit numbers of 320, 500, and 1,200, followed by a 1 μm diamond abrasive paste to ensure a smooth and uniform surface for all samples. The sample surfaces were pressed together with four rubber bands; each sample had four pieces pressed together as shown in Fig. 4. The width of the gap measured between the slices was approximately 40 μm. The pressed slices were partially submerged in DI water (approximately one-fourth the height of the samples) and allowed to heal in ambient condition for 14 days [Fig. 4(a)]. After the healing period, the pressed slices were separated and oven-dried at 55°C for 30 min. The healing products formed on the surfaces of the slices were gently scraped off with a blade and used in FTIR, TGA, and SEM.

FTIR

The FTIR spectra of the healing products scraped off from the surface of the sliced cement paste were characterized using a Perkin Elmer Paragon 1000 FTIR with an ATR accessory in the transmission mode. The healing products were passed through the sieve #60 to obtain a fine powder. Approximately 30 mg of the fine

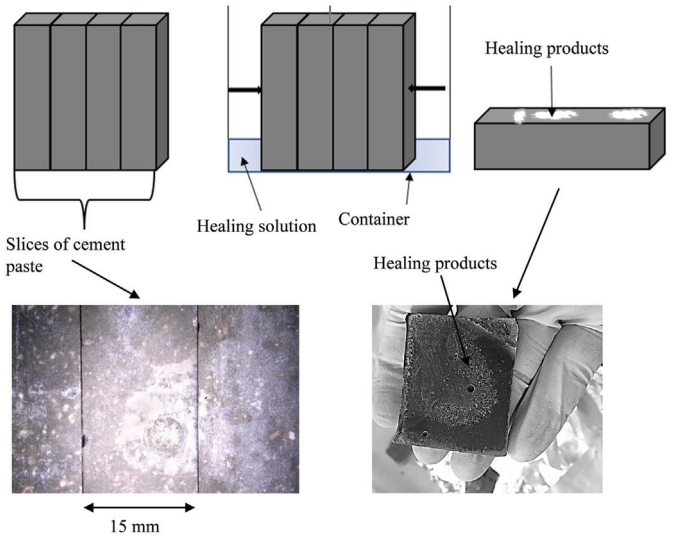

Fig. 4. Artificial planar cracks healed in various solutions.

powder was scanned at a resolution of 4 cm^{-1} in a spectra range of 600 to 4,000 cm^{-1}. Each sample was taken through four runs of scans, and the average is reported.

TGA

TGA was employed to investigate the mineralogical composition of the healing products formed on the sliced paste. Approximately 30 mg of the sample as prepared in FTIR was loaded into a Netzsch TG and scanned at a heating rate of 20°C/min and in the temperature range of 24°C to 900°C. The mass loss within the temperature range of 400°C to 500°C is assigned to the decomposition of CH, while the mass loss between 600°C and 750°C is attributed to the decomposition of $CaCO_3$. The content of CH and $CaCO_3$ was normalized with respect to the cement paste and quantified using Eqs. (2) and (3) below:

$$CH = (74.1 \times \Delta M)/(18 \times M) \quad (2)$$

$$CaCO_3 = (100.1 \times \Delta M)/(44 \times M) \quad (3)$$

where ΔM (mg) = mass change corresponding to CH or $CaCO_3$ decomposition; and M (mg) = initial mass of the sample.

SEM

The morphology and elemental composition of the healing products formed on the slice surfaces and in the cracked region were assessed using an SEM JEOL JSM-7000F equipped with EDX. For the crack region, approximately 25 mm^3 of the middle portion of the prisms containing the crack was cut and gold plated and imaged in an SEM. Gold coating was done to avoid charging. Images were taken at an accelerating voltage of 10 kV and at a working distance of 10 mm. The control, H, and H U-CP samples were used in SEM imaging of the crack region. Healing products formed on the surfaces of control slices and slices mixed with hydrogel containing urease were imaged.

Crack Filling

The crack filling in the cracked prisms after healing was examined using the Keyence optical microscope. The images were taken before and after healing to study the progress of healing with time. Optical images were taken on 0, 3, and 10 days of healing.

Mechanical Properties

Compressive Strength Regain. In order to assess the compressive strength regain resulting from self-healing, microcracks were introduced into the cement paste cubes by loading them up to the 90% of their respective ultimate compressive strength at the age of 21 days. The cubes were loaded in a SATEC mechanical testing machine. The choice of loading the cubes up to the 90% of the ultimate compressive strength was to generate stable microcracks in the samples. Jiang et al. (2015) also utilized 90% of the ultimate compressive strength to generate multiple cracks in cubic samples.

The cracked cubes were subjected to wet–dry cycles in both 0.5 M urea solution and DI water for 7 days to study the compressive strength regain. Another batch of samples was healed in DI water for 21 days. During one wet–dry cycle, the samples were partially placed in the solution for 1 h and subjected to dry condition for 23 h. After 7 and 21 days of healing corresponding to 7 and 21 wet–dry cycles, respectively, the compressive strength of the healed samples was determined. The compressive strength regain was determined using Eq. (4) shown below:

$$\text{Compressive strength regain} = C/C_o \quad (4)$$

where C = compressive strength of the cracked cubes healed for 7 or 21 days; and C_o = compressive strength of the uncracked cubes (V) cured for the total duration including the initial 21 days plus 7 or 21 days.

Flexural Strength Regain. Cement paste prisms were used to evaluate the effect of different hydrogels on the flexural strength regain of the prisms. The prisms were cured for 21 days and then subjected to a three-point bending load using an Instron 5966 testing machine (Instron, Norwood, MA, USA) to introduce a single crack starting at the middle of the bottom side of the prism. The load was applied on the sample at a rate of 0.05 mm/s until the crack reached the layer of glass fiber which was manifested by a sudden reduction in the load. After unloading, the crack width was measured to be about 0.08 to 0.1 mm. The presence of the layer of glass fiber ensures the same crack length and width in all prisms (Fig. 2). The cracked prisms used in the flexural strength test regain were healed in a wet–dry cycle condition for 21 days where the cracked portion of the samples was submerged in DI water for 1 h and then exposed to dry conditions for 23 h. The flexural strength regain was determined using Eq. (5) shown below:

$$\text{Flexural strength regain} = F/F_o \quad (5)$$

where F = flexural strength of the cracked prisms cured for 21 days and healed for another 21 days; and F_o = flexural strength of the uncracked prisms cured for 42 days.

Electrical Resistivity. The electrical resistivity of the uncracked cement paste cubes and healed cement paste cubes with or without hydrogels was evaluated using electrochemical impedance spectroscopy (EIS). The EIS test was performed using a Gamry 600 Potentiostat/Galvanosat (Gamry, Warminster, PA, USA). The test was conducted with an amplitude of 250 mV and a frequency range of 10^6 to 10 Hz. The test was conducted using the protocol described in (Vafaei et al. 2021). The electrical resistivity was determined using the following Eq. (6):

$$\rho = (Re)(A)/(t) \quad (6)$$

where ρ, Re, A, and t = electrical resistivity (Ω.m), measured resistance (Ω), surface area (m^2), and thickness (m) of the cubes, respectively.

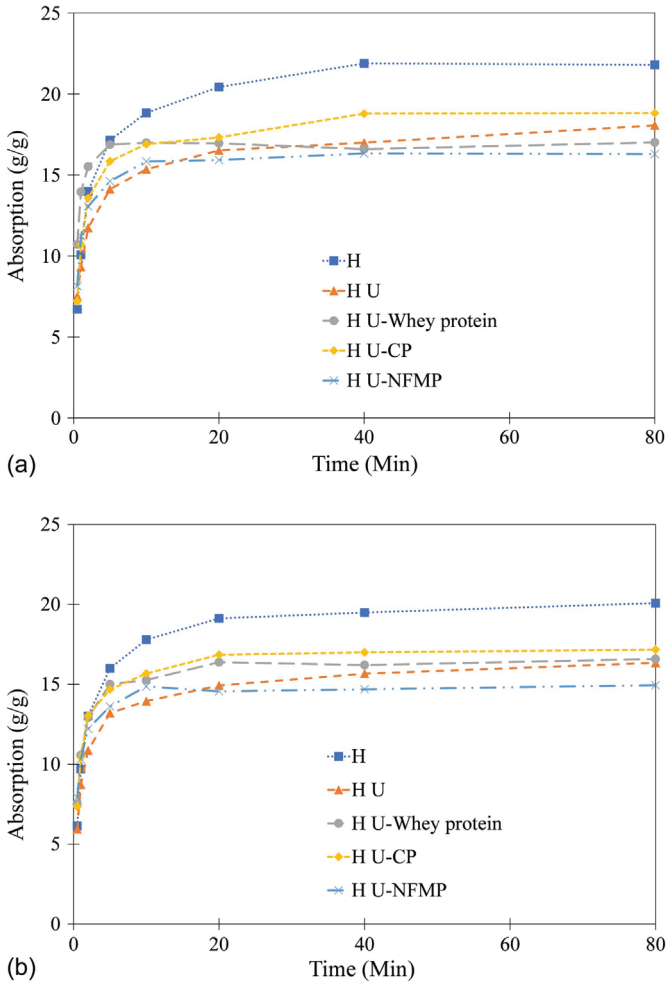

Fig. 5. Absorption of hydrogels in (a) 0.5 M $CaCl_2$; and (b) cement pore solution.

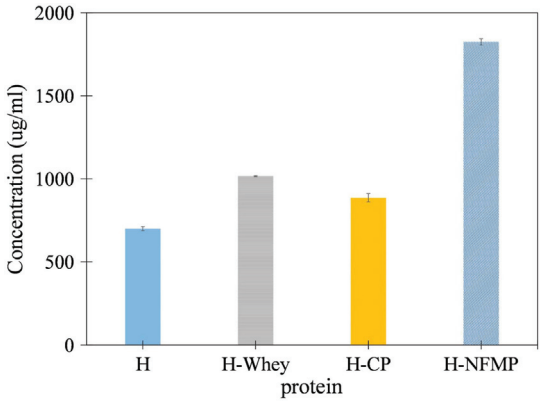

Fig. 6. Concentration of proteins released into the cementitious matrix surrounding the hydrogel microstrips.

Results and Discussion

Hydrogel Absorption

The absorption capacity of the different hydrogels in 0.5 M $CaCl_2$ and cement pore solution containing 1.5 M urea is illustrated in Fig. 5. It is seen that hydrogel absorption was fast at early stages and then slowed down and reached a plateau after 20 min. Generally, it can be observed that the absorption of hydrogels is slightly higher in the 0.5 M $CaCl_2$ solution [Fig. 5(a)] than in the cement pore solution [Fig. 5(b)]. This may be attributed to the pH difference between the two solutions and the difference in the ionic composition of the two solutions (Farzanian and Ghahremaninezhad 2018a, b; Kua et al. 2019; Li et al. 2019; Mignon et al. 2014; Prabahar et al. 2022; Schröfl et al. 2012; Zhu et al. 2015). The pH of the cement pore solution and the 0.5 M $CaCl_2$ was measured to be 12.5 and 9.5, respectively. At high pH of more than 12, the amide groups in the hydrogel polymer network hydrolyze to negatively charged carboxylate groups, which, in turn, increase the repulsive forces within the polymer network resulting in increased swelling and absorption (Zhu et al. 2015). On the other hand, in the presence of monovalent and multivalent cations such as Ca^{2+}, K^+, and Na^+, the absorption is reduced due to the screening effect and complexation between primarily Ca^{2+} and the negatively charged polymer backbone (Kang et al. 2017, 2018; Lee et al. 2018). The combined effect of pH and ionic composition determines the absorption behavior of the hydrogels.

It can be seen that the hydrogels containing urease and proteins showed lower water absorption in both media compared to hydrogel without urease or proteins (H). This is because H consists of 100% polymeric phase that can absorb solution while the hydrogels with urease and protein have slightly lower concentration of polymeric phase. Urease and proteins do not absorb solution. In addition, the presence of urease and proteins could provide a physical barrier for the polymer network expansion. The solutions contained urea, and upon absorption, a certain amount of urease inside the hydrogel hydrolyzed the urea into CO_3^{2-}, and in the presence of Ca^{2+} ions, $CaCO_3$ can be formed inside the hydrogel; thus, this can further constrain the polymer network expansion in the hydrogel.

Release of Protein into Cement Paste Matrix

The release of proteins from the hydrogels into surrounding matrix was investigated by measuring the presence of proteins using BCA. BCA has effectively been utilized to study the presence of protein in substances (Smith et al. 1985). After the cementitious matrix sets and the percolation of the solid skeleton in the matrix starts, the driving force for the release of solution from the hydrogel is dominantly the capillary suction (Farzanian and Ghahremaninezhad 2017). The role of the capillary forces in the desorption of hydrogels in a cementitious matrix and the underlying processes at the interface between the hydrogels and cementitious matrix were investigated in the previous studies (Farzanian and Ghahremaninezhad 2018a, 2017). Fig. 6 illustrates the concentration of proteins released into the cement matrix surrounding the hydrogel microstrip. It can be observed that H-NFMP exhibited the highest concentration of protein released into the cement matrix. The concentration of H-NFMP released into the cement matrix was twice as much as the concentration of H-whey protein released into the cement matrix. When exposed to hydrating cement paste, proteins can adsorb onto hydration products through either Ca^{2+} ion bridging or electrostatic interaction between negatively charged carboxylate group of the protein and the positively charged components of the hydration products of the cement particles (Liu et al. 2020; Mollah et al. 2000b). The result corresponding to H is likely due to the nonreacted amide presence in the hydrogel because the amide peaks also exist in crosslinked polyacrylamide hydrogels (Farzanian et al. 2021). Thus, the results provide evidence that proteins are able to be released from the hydrogels. The difference in the release

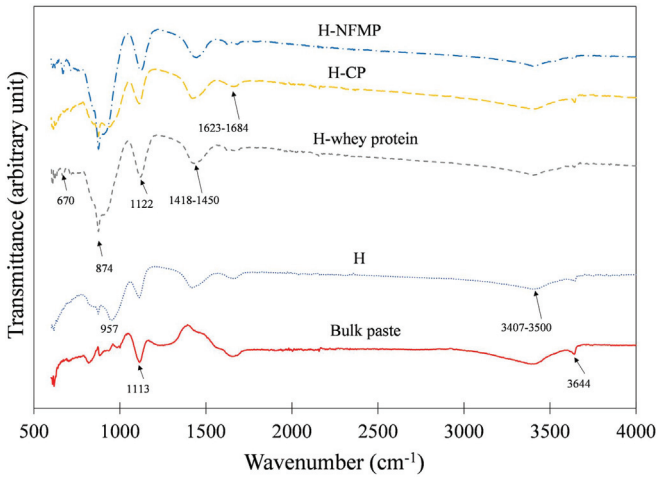

Fig. 7. FTIR of the cementitious matrix surrounding hydrogel microstrip.

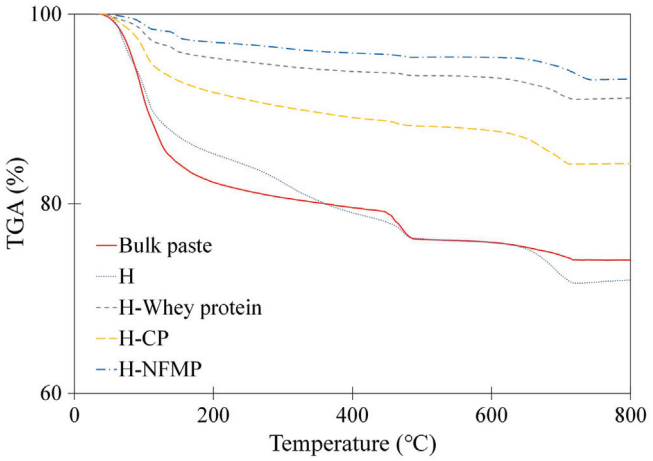

Fig. 8. TGA curve of cementitious matrix surrounding hydrogel microstrip.

amount of the proteins is related to the interactions between the proteins and the polymer network of the hydrogels.

Fig. 7 shows the FTIR results of the cement matrix surrounding the embedded hydrogel microstrip as depicted in Fig. 3. For comparison, the FTIR result of a sample from a region far away (bulk paste) from the hydrogel microstrip is also included in the figure. The peak located at 3,644 cm^{-1} for the bulk paste and the cementitious matrix surrounding hydrogels containing protein or hydrogel corresponds to the presence of CH (Yousuf et al. 1993). The intensity of the peak located at 3,644 cm^{-1} in the bulk paste indicated a higher content of CH in the bulk paste than in the surrounding matrix.

In addition, the broad band in the range of 3,407 and 3,500 cm^{-1} is assigned to the stretching vibration of hydroxyl groups (O—H) in H_2O (Huang et al. 2013). The peaks within the range of 1,623 and 1,684 cm^{-1} for the cementitious matrix surrounding H, H-CP, H-whey protein and H-NFMP are indicatives of carboxylate stretching from the acrylamide in the hydrogel (Farzanian et al. 2019; Magalhães et al. 2012; Mignon et al. 2014) and the bending deformation of the primary amide in protein (Mignon et al. 2015). Furthermore, the peak located at 874 cm^{-1} and bands in the range of 1,418 to 1,450 cm^{-1} are assigned to the out-of-plane bending of CO_3^{2-} (Xia et al. 2015) and asymmetric stretching of CO_3^{2-} (Huang et al. 2013), respectively. The appearance of this peak and bands demonstrated the presence of $CaCO_3$ in the cementitious matrix surrounding the hydrogel. The solution released from the hydrogel into the surrounding matrix contained dissolved CO_2, which facilitates the conversion of CH to $CaCO_3$. Apparently, this peak and band were weak in the bulk paste. All FTIR spectra showed additional peaks at 1,113 and 957 cm^{-1} corresponding to the presence of ettringite (Mollah et al. 2000a) and the Si—O stretching vibration in C—S—H gel, respectively (Huang et al. 2013; Kamali and Ghahremaninezhad 2018a, b). The Si—O stretching vibration appeared not distinct from the CO_3^{2-} peak at 874 cm^{-1} in the cementitious matrix surrounding the hydrogels. Comparing the intensities and positions of the Si-O stretching vibrations, the peak was more intense and shifted more to the right in the case of the cementitious matrix surrounding the hydrogels with proteins compared to the sample with H or the matrix far away (bulk paste) from the hydrogel microstrips. For instance, whereas the Si—O stretching vibrations showed up at 1,113 cm^{-1} in the bulk paste and H, it shifted to 1,122 cm^{-1} in the cementitious matrix with H-NFMP, H-whey protein, and H-CP. This could be an indication of the interaction between the released protein and ettringite, since proteins have higher affinity toward ettringite (Baffoe and Ghahremaninezhad 2022a, b).

Fig. 8 shows the TGA profile of the matrix surrounding the embedded hydrogel microstrip and the matrix far away (bulk paste) from the hydrogel microstrip. The mass loss at the temperature below 100°C corresponds to the loss of weakly bound water, which is physically adsorbed on the solid gel (Esteves 2011). The mass loss that occurred in the temperature of 110°C to 200°C corresponds to the dehydroxylation of the C—S—H gel (Esteves 2011; Lothenbach et al. 2012). In addition, there is a noticeable mass loss in the temperature range of 420°C and 480°C, which can be attributed to the decomposition of CH (Esteves 2011). The mass loss that occurred in the temperature range of 420°C and 480°C was more pronounced in the H sample compared to the hydrogels containing proteins, and this will be discussed in the next section. Furthermore, when the temperature increased from 651°C to 721°C, there was a significant mass loss in the TGA profile. This mass loss is attributed to the decomposition of $CaCO_3$ (Pane and Hansen 2005; Ye et al. 2007). Comparing the information obtained from the FTIR and TGA analyses, it can be concluded that the main products formed around the embedded hydrogel are C-S-H, ettringite, CH, and $CaCO_3$.

The quantification of the CH and $CaCO_3$ contents of the cementitious matrix surrounding the hydrogels is shown in Fig. 9. It is noticed that the matrix surrounding the hydrogel microstrip showed a higher content of $CaCO_3$ compared to the far away region, which is in support of the FTIR results shown in Fig. 7. Among the hydrogel samples, the highest percentage of $CaCO_3$ was noticed in H, with H-whey protein and H-NFMP showing the least $CaCO_3$. A similar trend was noticed in the CH content. This could be explained in light of the fact that the presence of water released from the hydrogel aided in the continued hydration and hence formation of more hydration products (Snoeck et al. 2014a). As observed in the absorption experiment in Fig. 5, H showed higher solution absorption compared to the other hydrogels and as such would have the capacity to release more water into the surrounding cementitious matrix during desorption. It is therefore interesting to note that H-CP, which had a higher solution absorption capacity, showed higher content of CH and $CaCO_3$ compared to H-whey protein and H-NFMP. In addition to the lower absorption capacity, the surface adsorption of the released proteins onto surrounding cementitious matrix could reduce surface area for hydration reaction and hence

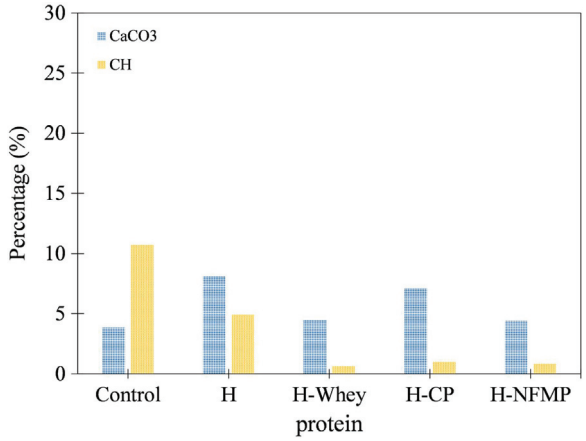

Fig. 9. TGA quantification of the cementitious matrix surrounding hydrogel microstrip.

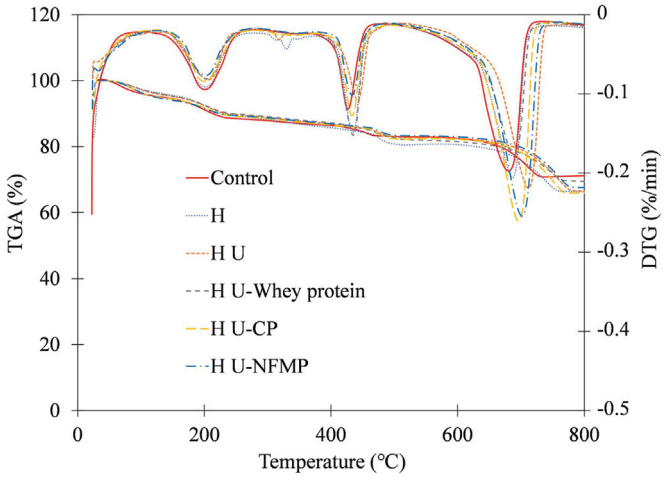

Fig. 11. TGA curve of healing products scraped from the surfaces of healed sliced cement paste.

lead to the formation of a smaller amount of hydration products (Baffoe and Ghahremaninezhad 2022b). This result is consistent with the findings of the release test discussed in Fig. 6.

Characterization of the Healing Products in Cement Paste with Hydrogels Containing Urease and Proteins

FTIR

The FTIR spectra of healing products formed on the surface of the cement paste slice as described in Fig. 4 are shown in Fig. 10. The sharp in-plane bending (v_4) peak at 712 cm^{-1} and out-of-plane bending peak at 874 cm^{-1} correspond to the presence of calcite (Baffoe and Ghahremaninezhad 2023; Delgado et al. 1996; Weir and Lippincott 1961). All samples showed a peak at 966 cm^{-1}, corresponding to the stretching vibration of Si—O in C—S—H (Ghosh and Handoo 1980). The characteristic band in the range of 1,155 to 1,160 cm^{-1} of the control and the hydrogel modified samples corresponds to the S—O stretching vibration of SO_4^{2-}, which could be due to the presence of ettringite (Mollah et al. 2000a; Ylmén et al. 2009). Furthermore, the band located at 1,413 cm^{-1} corresponds to the asymmetric stretching of CO_3^{2-} providing evidence for the presence of $CaCO_3$. The O—H of water and amide I both showed peaks at 1,643 cm^{-1} (Hughes et al. 1995; Valenzuela et al. 2013); however, the 1,643 cm^{-1} peak appeared to be relatively weaker in the control sample compared to the 1,643 cm^{-1} in the samples mixed with hydrogels. The strength of the peaks in the samples mixed with hydrogel and/or proteins is attributed to the combined effect of the O-H from water and amide I from the hydrogel, proteins, and urea (Gallagher 1958; Yang et al. 2006; Ylmén et al. 2009). All these samples exhibited a broad but weak band in the range of 3,362–3,472 cm^{-1}, corresponding to the O—H band due to the presence of bound water (Huang et al. 2013). The peak at 3,647 cm^{-1} is attributed to the presence of CH in the healing products (Yousuf et al. 1993) while the peak at 1,797 cm^{-1} indicates the presence of $CaCO_3$ (Baffoe and Ghahremaninezhad 2022b).

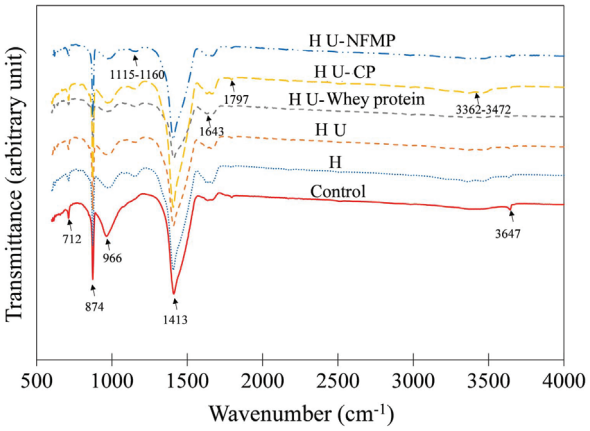

Fig. 10. FTIR of the healing products corresponding to different samples.

TGA/DTG

Fig. 11 illustrates the TGA/DTG curves of the healing products formed on the surface of the paste slices. The mass loss at 200°C corresponds to the loss of chemically bound water from C-S-H and possible decomposition of excess organic molecule (urea) (Baffoe and Ghahremaninezhad 2022a). H and H U showed additional mass losses between 317°C and 330°C, indicative of the decomposition of amides (Khan et al. 2021). As the temperature increased, a noticeable mass loss occurred between 408°C and 460°C. This mass loss is attributed to the decomposition of CH (Baffoe and Ghahremaninezhad 2022a; Huang et al. 2013; Ye et al. 2007). Moreover, a major mass loss occurred between 640°C and 740°C with the control showing the least peak. This mass loss is attributed to the decomposition of $CaCO_3$ (Baffoe and Ghahremaninezhad 2022a). The CH and $CaCO_3$ contents are shown in Fig. 12. It can be seen that the content of $CaCO_3$ in the samples containing hydrogel or hydrogel urease/protein is higher than in the control sample (without hydrogel). This observation suggests that provision of water from the hydrogel increased $CaCO_3$ formation. The higher content of $CaCO_3$ in the paste with hydrogels containing urease compared to the paste with H can be due to the fact that in the presence of CO_3^{2-} released due to urea decomposition by urease, the dissolution of Ca^{2+} from CH can further react with the CO_3^{2-} to promote the formation of $CaCO_3$ (Dakhane et al. 2018). This is reflected in the lower content of CH in the samples with hydrogels containing urease. Considering the FTIR peaks in Fig. 10, it appears that the dominant polymorph of the $CaCO_3$ was calcite as indicated by the strong intensities of 712 cm^{-1} in H U, H U-CP, and H U-NFMP. Interestingly, the H U-whey protein, which showed lower content of $CaCO_3$, exhibited a relatively weaker

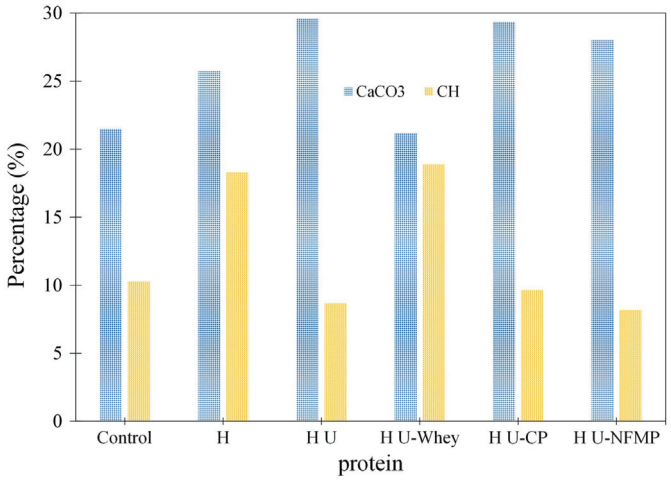

Fig. 12. TGA quantification of the healing products.

peak corresponding to calcite in the FTIR results in Fig. 10. The formation of calcite as the dominant polymorph in the hydrogel with urease is consistent with prior results, which stipulates that urease induced calcite formation is favored when precipitation occurs near or on cementitious surfaces (Baffoe and Ghahremaninezhad 2022a). The slightly lower content of $CaCO_3$ in the H U-whey protein could be due to lower release of urease from this hydrogel. The slightly higher CH content in the case of H U-whey protein could attest to the lower enzymatic activities in the case of this hydrogel.

SEM

Fig. 13 shows the SEM images of the healing products formed on the surfaces of the control slice, the slice of cement paste mixed H, and the slice of cement paste mixed H U described in Fig. 4. The SEM of the slices mixed with H U was used as a representative of all other slices mixed with urease because they showed similar features. The SEM of the healing products formed on the surface of the control slices shown in Fig. 13(a) revealed the formation of hexagonal shaped platelets noted as CH and phases indicating the presence of $CaCO_3$ (Baffoe and Ghahremaninezhad 2022b). The formation of these phases matches the findings of the FTIR in Fig. 10. Shown in Fig. 13(c) is the SEM of the healing products formed on the surface of the slices mixed with H U. A larger amount of $CaCO_3$ is observed in this image compared to Fig. 13(a). The higher content of $CaCO_3$ is attributed to the enzymatic reaction as well as the contribution of the hydrogels (Baffoe and Ghahremaninezhad 2022a). The absence or low amount of CH in the SEM of the slices mixed with H U is consistent with the findings of the FTIR and TGA in Figs. 10 and 12.

Crack Filling

Fig. 14 shows the crack filling process using optical microscopy at the time intervals of 0, 3, and 10 days of healing. Generally, the crack area of the various samples reduced with the healing time. It is noticed that the control sample showed no significant crack healing after the 10-day healing period while the samples mixed with H showed partial crack closure after 10 days. It can be observed that the samples mixed with hydrogels containing urease/urease proteins showed complete crack closure after the 3- and 10-day healing period.

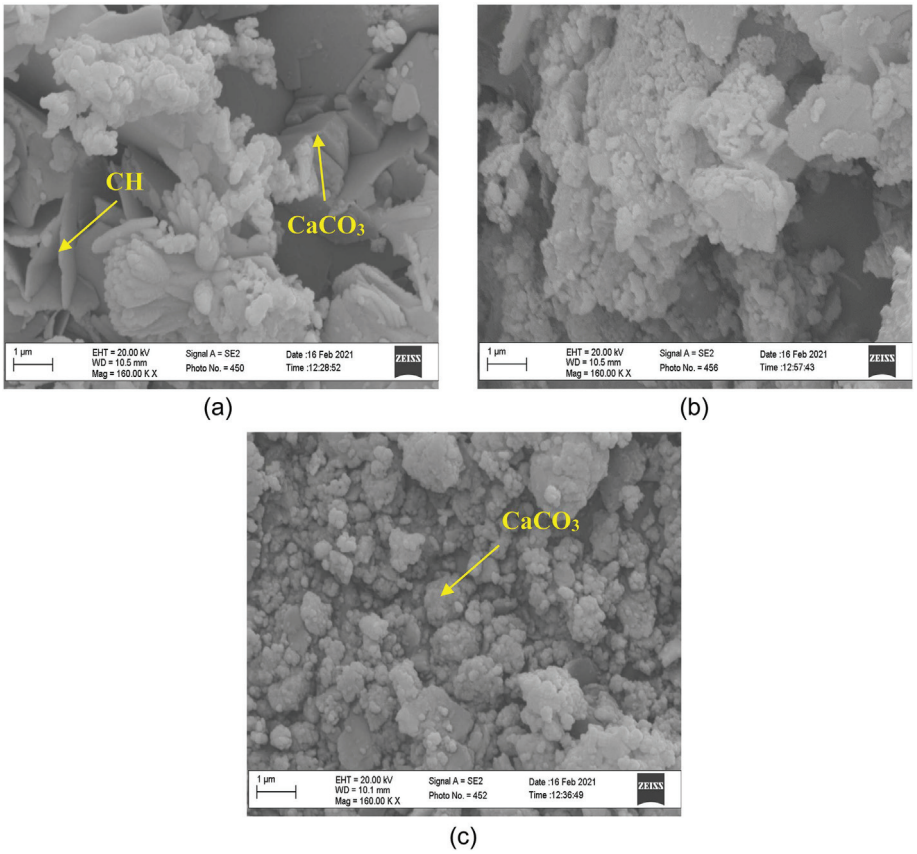

Fig. 13. SEM of the healing products formed on the surfaces of (a) control slice; (b) slice mixed with H; and (c) slice mixed with H U.

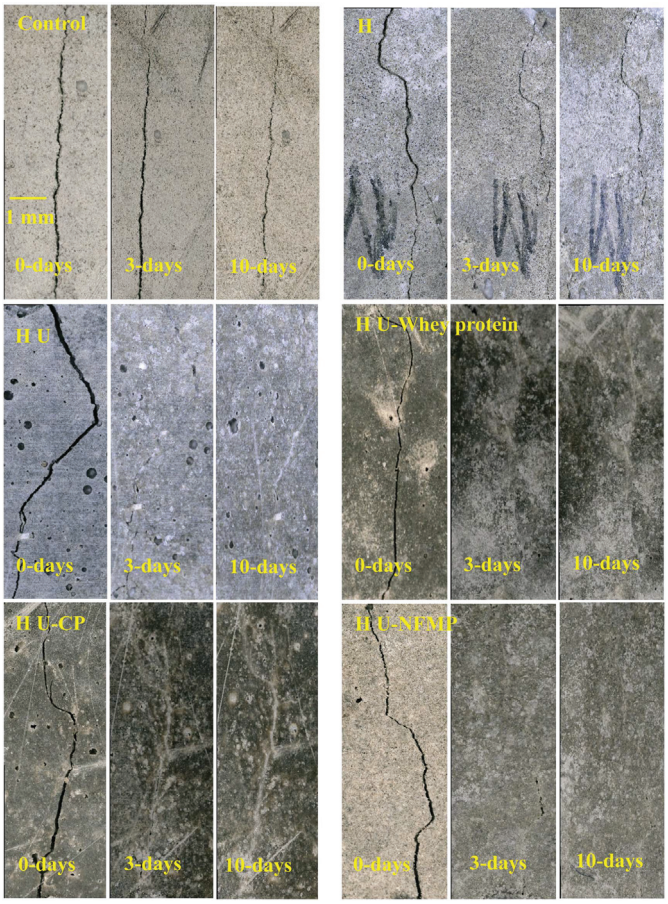

Fig. 14. Optical images of cracked prism samples healed in DI water. The scale bar is the same for all images and corresponds to 1 mm.

Shown in Fig. 15 are the SEM images and EDX analysis of the healing materials formed in the cracks of healed samples after 10 days of healing period. Images from the SEM revealed an unhealed crack area and partial crack-healed area in the control and the sample mixed with hydrogel (H), respectively. In the case of samples mixed with H U-CP it can be observed that there was a significant closure of the cracked area. The EDX analysis of the region marked with a yellow box confirmed that calcium, carbon, and oxygen constituted about 90% of the healing products in the crack indicating $CaCO_3$ as a primary phase in the healing products formed in the cracks.

The healing mechanism observed when studying the cracked samples in the wet and dry cycles can be grouped into multiple factors; these are $CaCO_3$ crystallization due to the enzymatic action and a combination of continued hydration and $CaCO_3$ crystallization. The observed partial crack closure in the control samples and the sample with H, after the 10-day healing period, can be attributed to continued hydration of the unreacted part of the cement and $CaCO_3$ crystallization due to the presence of dissolved CO_2 in the crack space. It is seen that the crack closure is more pronounced in the case of H, which is due to the ability of hydrogels to retain water during the wet condition and to gradually release water during the dry condition to allow the hydration and $CaCO_3$ formation to occur. Although enough moisture is available during the wet healing cycle, the control cement paste could not retain much moisture as the absorbed water evaporated during the dry cycle, thereby showing partial crack closure (Kua et al. 2019; Wang et al. 2014a).

The complete healing of cracks in the samples mixed with H U and proteins can be attributed to the improved autogenous healing due to the activity of the hydrogel (Snoeck et al. 2014a) and the $CaCO_3$ precipitation due to the enzymatic action (Baffoe and Ghahremaninezhad 2022a). As the wet healing cycle proceeded, enough moisture was retained, which may be absorbed by the hydrogel. When left to dry, the retained moisture is released into the cementitious matrix for the continued reaction (Snoeck and De Belie 2016). The EICP is a quick process and proceeds when the necessary conditions are met (Baffoe and Ghahremaninezhad 2022a). As the urease is released from the hydrogel during the wet and dry cycle, it reacts with the available urea and Ca^{2+} to form $CaCO_3$, which fills the cracks and enables the crack to heal (Baffoe and Ghahremaninezhad 2022a). Due to their rapid nature, EICP has been employed to treat surface cracks of concrete materials, making it attractive for infrastructural repairs (Baffoe and Ghahremaninezhad 2022a; Dakhane et al. 2018). It should be borne in mind that the microscopy observations made here correspond to the surface of the crack and could be different from the crack deep inside the samples.

Compressive Strength Regain

Fig. 16 illustrates the compressive strength of the virgin samples (V) at 28 and 42 days and the strength regain after the cracked samples were healed in urea and DI water for 7 and 21 days. It should be noted that the samples were cracked at the age of 21 days. The compressive strength regain of the samples corresponding to 7 days and 21 days of healing is demonstrated in Fig. 17. As shown in Fig. 16, the samples mixed with hydrogels exhibited lower initial compressive strength, and this may be attributed to the formation of macrovoids in the cementitious matrix, which act as stress concentration sites in the microstructure, thus reducing the overall compressive strength of the samples. Previous studies have reported the reduction of compressive strength due to the addition of hydrogels (Farzanian et al. 2016a; Li et al. 2019; Schröfl et al. 2012; Snoeck et al. 2014a; Vafaei et al. 2021). Among the samples with hydrogels, H U-NFMP showed a relatively higher virgin compressive strength, and this could be attributed to the lower absorption of H-NFMP compared to the other hydrogels as revealed in Fig. 5. Due to the lower water absorption, it is expected that the size of macrovoids formed in the cement paste sample mixed with H U-NFMP was comparatively smaller, thus lowering the stress concentration effect in the microstructure. It is noted that the effect of hydrogel in reducing the virgin compressive strength of the cement paste followed the hydrogels' trend of solution absorption as shown in Fig. 5.

After healing in various solutions, it is observed that the healed control sample showed a lower compressive strength compared to the uncracked (V) control sample. Interestingly, in the samples with hydrogel containing urease or urease and proteins, the healed sample demonstrated a higher compressive strength compared to the uncracked sample indicating better self-healing performance. In the case of the sample with H, the cracked sample exhibited a similar compressive strength compared to the uncracked sample indicating regain of strength due to self-healing. The higher compressive strength regain of the samples mixed with hydrogels containing urease and urease/proteins compared to the sample with hydrogel only is attributed to the formation of a larger amount of healing products in the crack space due to enzymatic reaction. This is in agreement with the crack filling results as shown in Fig. 14. It is noted that healing in DI water or urea seemed to have a similar strength regain effect in all samples. Given the large scatter in the case of H U-whey protein and H U-CP, healed in DI water,

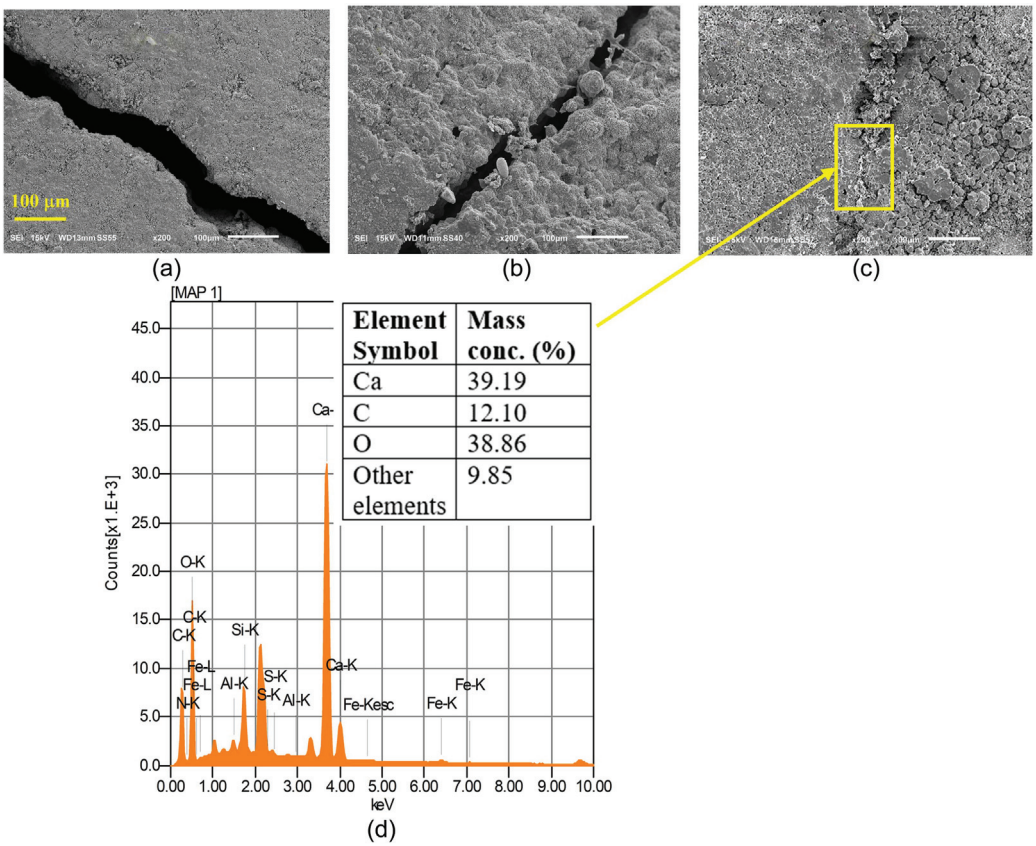

Fig. 15. SEM image of the crack in (a) control sample and the samples with (b) H; and (c) H U-CP, respectively. (d) EDS analysis corresponding to the area marked in (c). The scale bar is the same for all SEM images. The letters K and L refer to the different electron shells in element atoms.

the difference in strength regain between the samples healed in DI water and in urea in the case of these two proteins is not significant.

As seen in Fig. 17, the compressive strength regain of H U-whey protein, H U-CP, and H U-NFMP was approximately 1.2 and was higher than the strength regain of the sample with H U. A comparison of the $CaCO_3$ content of the sample with H U to the samples containing H U-whey protein, H U-CP, and H U-NMFP (Fig. 12) indicates a small difference in the $CaCO_3$ between these samples. Thus, the difference in the amount of $CaCO_3$ is not likely to be the reason for increased strength regain of the samples with hydrogels that have proteins. The improved strength regain of the healed cracked samples with hydrogels containing proteins can be attributed to the interfacial bond contributed by the released proteins. The proteins are able to bind together the solid constituents of the healing products and also bind the healing products to the surfaces of the cracks, thereby improving the overall strength of the samples. The negatively charged functional groups of the proteins can be crosslinked in the presence of Ca^{2+}, leading to the densification

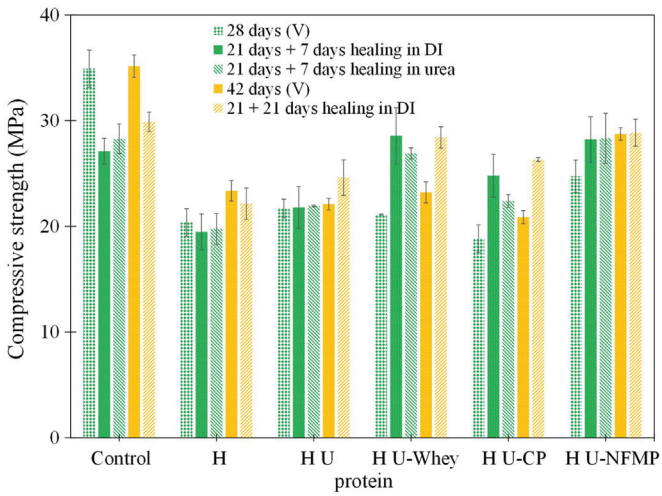

Fig. 16. Compressive strength of uncracked (V) and healed cracked samples.

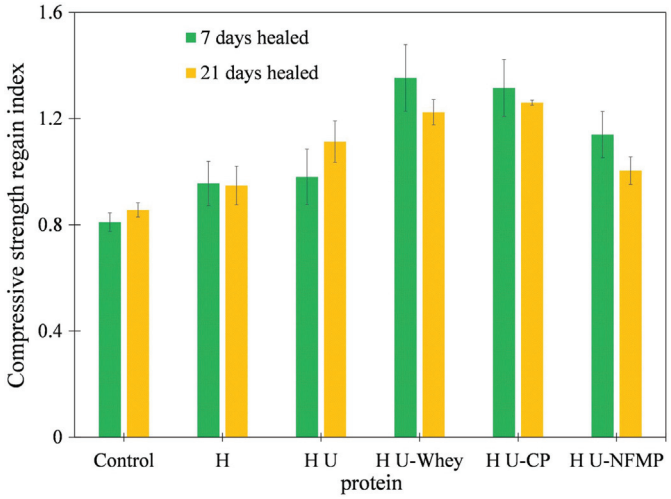

Fig. 17. Compressive strength regain index of the samples healed in DI water.

of the microstructure and enhancement of interfacial bonds of the healing products.

The interfacial bond of proteins to cementitious materials and calcium carbonate has been investigated in the past (Baffoe and Ghahremaninezhad 2022a, b). The ability of the biomolecule to enhance mechanical properties through the formation of organic–inorganic hybrid phases has also been investigated in systems containing calcium carbonate as a primary binding phase (Khan et al. 2021, 2023). It should be noted that macrovoids are created in the microstructure as a result of hydrogel absorption and then desorption (De Belie et al. 2018; Farzanian et al. 2016b; Kamali and Ghahremaninezhad 2017; Mechtcherine and Reinhardt 2012; Snoeck et al. 2015; Wehbe and Ghahremaninezhad 2017). These macrovoids act as weak sites in the matrix, promoting formation of multiple small cracks rather than one large crack (Lee et al. 2010; Mignon et al. 2017; Snoeck et al. 2014b). Since hydrogels are likely to be present on the crack path, they can more effectively facilitate the healing process of the cracks.

Flexural Strength Regain

The flexural strength regain of different samples is shown in Fig. 18. Samples with hydrogel containing urease/protein exhibited higher flexural strength regain while the control showed the lowest flexural strength regain. The results of the flexural strength regain are consistent with the results of the compressive strength regain. However, it is noted that the enhancement in regain in flexural strength is more pronounced compared to that in compressive strength when comparing the control samples with other samples. As discussed, the released proteins enhanced the interfacial bond between the healing products at the micro and nanoscales (cohesion) and between the healing products and the crack surface (adhesion), ultimately improving the strength regain. The results presented here are in good agreement with the prior work (Baffoe and Ghahremaninezhad 2022a) focused on the influence of proteins on consolidating and binding loose ground cementitious particles. The effect of increased interfacial bond provided by proteins on enhancing flexural strength was also evidenced in our prior work (Baffoe and Ghahremaninezhad 2022a). Fig. 19 shows a schematic of the interfacial bond between solid phases in the microstructure provided by the proteins.

Electrical Resistivity

Electrical resistivity has been used as a measure of the transport properties of cementitious materials (Bazhuni et al. 2019; Farzanian et al. 2016a, 2021; Flores et al. 2015, 2017; Kamali and Ghahremaninezhad 2015, 2017; Neithalath et al. 2006; Vafaei et al. 2020). The electrical resistivity of cement paste is controlled by the pore structure and pore solution chemistry (Bu and Weiss 2014; Jain and Neithalath 2011). Fig. 20 illustrates the electrical resistivity of uncracked (V) and healed samples at different ages (7 and 21 days). From the test result, it is seen that the electrical resistivity of the samples with hydrogels was lower at the uncracked state compared to that of the control. The lower electrical resistivity of uncracked samples containing hydrogels is potentially because the hydrogels act as electrical conductors decreasing the total electrical resistivity of the cement pastes (Farzanian et al. 2021). After 7 days of healing, while the control sample showed a similar electrical resistivity compared to the uncracked sample, most of the samples with hydrogels showed a higher electrical resistivity compared to the respective uncracked sample. All samples showed an increase in electrical resistivity in the samples after 21 days of healing, and this increase is more pronounced in the sample with hydrogels containing proteins. The increase in electrical resistivity in the healed samples is attributed to the crack filling as well as an increase in microstructure densification in the matrix with time. Assuming a relatively similar contribution from the latter mechanism, it is reasonable to stipulate that the difference in increase in electrical resistivity of the samples is mainly due to the crack filling process. It is interesting to note that the electrical resistivity and mechanical strength regain of the samples follow a similar trend. The samples with hydrogels containing proteins demonstrated markedly higher improvement in crack filling compared to the control samples, and this improvement appeared to be more pronounced in the samples with hydrogels and proteins. The sample with H U did not show an

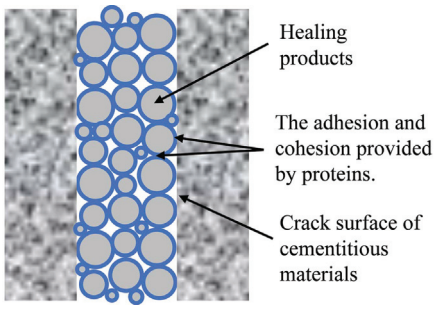

Fig. 19. Schematic illustrating the cohesion and adhesion provided by the proteins in the microstructure of the healing products.

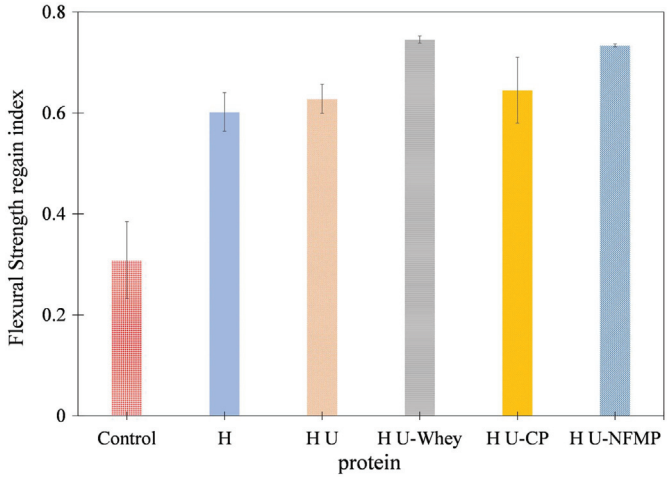

Fig. 18. Flexural strength regain index of the healed samples.

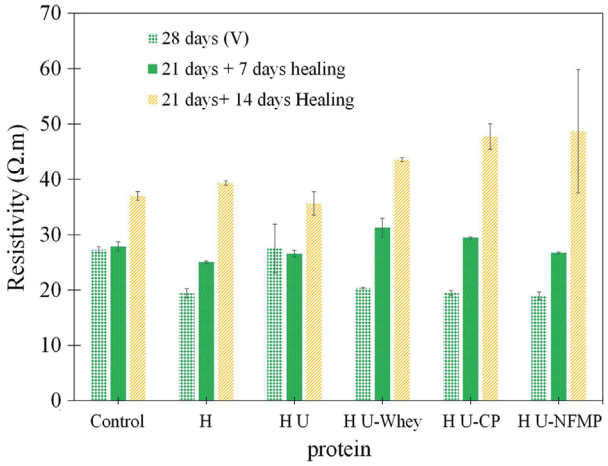

Fig. 20. Electrical resistivity of the healed samples.

improvement compared to the sample with hydrogel only (H). Overall, the electrical resistivity results could provide further evidence of the positive influence of the proteins on the healing process of the cement paste samples.

Conclusions

In this study, the self-healing effect of hydrogels containing urease and three different proteins in cracked cementitious materials was investigated. The findings from this study are as follows:

- The encapsulation of proteins and urease slightly decreased the absorption capacity of the hydrogel possibly due to increased constraints in the polymer network of the hydrogels as a result of interaction with proteins and urease.
- It was shown that proteins can be released to different degrees from the hydrogels into the surrounding cementitious matrix. TGA and FTIR indicated a change in the chemical composition in the region surrounding hydrogels compared to the region far away from the hydrogel. This is attributed to released water and the interaction between proteins and surrounding cementitious matrix.
- TGA and FTIR showed increased calcium carbonate in the healing products in the cement paste containing different hydrogels compared to the control cement paste. Among the cement pastes with hydrogels, the hydrogels containing urease and protein resulted in slightly higher calcium carbonate content due to the enzymatic reaction. Calcite was found to be the dominant calcium carbonate polymorph.
- The optical and SEM imaging showed enhanced crack filling in the samples mixed with hydrogels due to improved autogenous healing. The samples mixed with hydrogel containing urease and protein were shown to exhibit marked improvement in crack filling as a result of the enzymatic reaction.
- The mechanical strength results indicated a noticeable increase in the mechanical strength regain in the samples with hydrogels containing proteins, and this increase was more noticeable in the flexural strength regain. The improved mechanical strength regain is attributed to enhanced interfacial strength between solid phases in the healing products at the microstructure level. As a result, the cohesion within healing products and the adhesion between the healing products and cracked surface is improved leading to increased mechanical strength regain.
- The cracked samples mixed with hydrogel containing urease and protein were shown to exhibit markedly higher strength regain compared to the control and the samples mixed with hydrogel only. The increased strength regain could be in part due to the crack healing by the precipitated $CaCO_3$ and the stronger interfacial bond between crack surfaces due to the adhesive effect of the released proteins.
- The electrical resistivity results were in agreement with the mechanical strength regain exhibiting increased resistivity in the healed samples with hydrogels containing proteins.

It should be noted that this paper focuses on cement paste of relatively young age; further research is needed to explore the proposed self-healing method for cement paste of longer age.

Data Availability Statement

Some or all data, models, or code that support the findings of this study are available from the corresponding author upon reasonable request.

Acknowledgments

This study was supported in part by the National Science Foundation under the CAREER award number 1846984. Any opinions, findings, and conclusions or recommendations expressed in this material are those of the author(s) and do not necessarily reflect the views of the National Science Foundation.

References

Aldea, B. C., W. Song, J. S. Popovics, A. Member, and S. P. Shah. 2000. "Extent of healing of cracked normal strength concrete." *J. Mater. Civ. Eng.* 12 (Feb): 92–96. https://doi.org/10.1061/(ASCE)0899-1561(2000)12:1(92).

Almajed, A., H. K. Tirkolaei, E. Kavazanjian, and N. Hamdan. 2019. "Enzyme induced biocementated sand with high strength at low carbonate content." *Sci. Rep.* 9 (1): 1–7. https://doi.org/10.1038/s41598-018-38361-1.

Arriaga, T. V. 2011. "Controlled and tailored denaturation and aggregation of whey proteins Tatiana Vieira Arriaga Engenharia Biológica Júri." Master thesis, Instituto de Bioengenharia e Biociências, Instituto Superior Técnico.

Baffoe, E., and A. Ghahremaninezhad. 2022a. "The effect of biomolecules on enzyme-induced calcium carbonate precipitation in cementitious materials." *Constr. Build. Mater.* 345 (Aug): 128323. https://doi.org/10.1016/j.conbuildmat.2022.128323.

Baffoe, E., and A. Ghahremaninezhad. 2022b. "On the interaction between proteins and cracked cementitious surface." *Constr. Build. Mater.* 352 (Oct): 128982. https://doi.org/10.1016/j.conbuildmat.2022.128982.

Baffoe, E., and A. Ghahremaninezhad. 2023. "Effect of proteins on the mineralization, microstructure and mechanical properties of carbonation cured calcium silicate." *Cem. Concr. Compos.* 141 (Feb): 105121. https://doi.org/10.1016/j.cemconcomp.2023.105121.

Bazhuni, M. F., M. Kamali, and A. Ghahremaninezhad. 2019. "An investigation into the properties of ternary and binary cement pastes containing glass powder." *Front. Struct. Civ. Eng.* 13 (3): 741–750. https://doi.org/10.1007/s11709-018-0511-5.

Bian, H. 2012. "Colloidal behavior of casein biopolymer in alkaline solution and its application in self-levelling underlayments (SLUs)." Doctoral dissertation, Faculty of Chemistry, Technische Universität München.

Black, A. P. 2022. *2022 bridge report*. Washington, DC: American Road and Transportation Builders Association.

Briegel, C., H. Coelfen, and J. Seto. 2012. "Single amino acids as additives modulating $CaCO_3$ mineralization." *Adv. Topics Biomineralization* 33 (Feb): 33–48. https://doi.org/10.5772/39297.

Bu, Y., and J. Weiss. 2014. "The influence of alkali content on the electrical resistivity and transport properties of cementitious materials." *Cem. Concr. Compos.* 51 (Feb): 49–58. https://doi.org/10.1016/j.cemconcomp.2014.02.008.

Chindasiriphan, P., H. Yokota, and P. Pimpakan. 2020. "Effect of fly ash and superabsorbent polymer on concrete self-healing ability." *Constr. Build. Mater.* 233 (Jan): 116975. https://doi.org/10.1016/j.conbuildmat.2019.116975.

Costa, O. Y. A., J. M. Raaijmakers, and E. E. Kuramae. 2018. "Microbial extracellular polymeric substances: Ecological function and impact on soil aggregation." *Front. Microbiol.* 9 (Jul): 1–14. https://doi.org/10.3389/fmicb.2018.01636.

Dakhane, A., et al. 2018. "Crack healing in cementitious mortars using enzyme-induced carbonate precipitation: Quantification based on fracture response." *J. Mater. Civ. Eng.* 30 (4): 04018035. https://doi.org/10.1061/(ASCE)MT.1943-5533.0002218.

De Belie, N., et al. 2018. "A review of self-healing concrete for damage management of structures." *Adv. Mater. Interfaces* 5 (17): 1800074. https://doi.org/10.1002/admi.201800074.

Delgado, A. H., R. M. Paroli, and J. J. Beaudoin. 1996. "Comparison of IR techniques for the characterization of construction cement minerals and hydrated products." *Appl. Spectrosc.* 50 (8): 970–976. https://doi.org/10.1366/0003702963905312.

Edvardsen, C. 1999. "Water permeability and autogenous healing of cracks in concrete." *ACI Mater. J.* 96 (4): 448–454.

Espinosa, H. D., A. L. Juster, F. J. Latourte, O. Y. Loh, D. Gregoire, and P. D. Zavattieri. 2011. "Tablet-level origin of toughening in abalone shells and translation to synthetic composite materials." *Nat. Commun.* 2 (1): 173. https://doi.org/10.1038/ncomms1172.

Esteves, L. P. 2011. "On the hydration of water-entrained cement-silica systems: Combined SEM, XRD and thermal analysis in cement pastes." *Thermochim. Acta* 518 (1–2): 27–35. https://doi.org/10.1016/j.tca.2011.02.003.

Fahimizadeh, M., A. D. Abeyratne, L. S. Mae, R. K. R. Singh, and P. Pasbakhsh. 2020. "Biological self-healing of cement paste and mortar by non-ureolytic bacteria encapsulated in alginate hydrogel capsules." *Materials* 13 (17): 3711. https://doi.org/10.3390/ma13173711.

Farzanian, K., et al. 2016a. "The mechanical strength, degree of hydration, and electrical resistivity of cement pastes modified with superabsorbent polymers." *Constr. Build. Mater.* 109 (Aug): 156–165. https://doi.org/10.1016/j.conbuildmat.2015.12.082.

Farzanian, K., and A. Ghahremaninezhad. 2017. "The effect of the capillary forces on the desorption of hydrogels in contact with porous cementitious material." *Mater. Struct.* 50 (5): 216. https://doi.org/10.1617/s11527-017-1068-9.

Farzanian, K., and A. Ghahremaninezhad. 2018a. "Desorption of superabsorbent hydrogels with varied chemical compositions in cementitious materials." *Mater. Struct.* 51 (Feb): 1–15. https://doi.org/10.1617/s11527-017-1128-1.

Farzanian, K., and A. Ghahremaninezhad. 2018b. "On the effect of chemical composition on the desorption of superabsorbent hydrogels in contact with a porous cementitious material." *Gels* 4 (3): 70. https://doi.org/10.3390/gels4030070.

Farzanian, K., and A. Ghahremaninezhad. 2018c. "On the interaction between superabsorbent hydrogels and blended mixtures with supplementary cementitious materials." *Adv. Civ. Eng. Mater.* 7 (4): 1–24. https://doi.org/10.1520/ACEM20180073.

Farzanian, K., K. Pimenta Teixeira, I. Perdiago Rocha, L. De Sa Carneiro, and A. Ghahremaninezhad. 2016b. "The mechanical strength, degree of hydration, and electrical resistivity of cement pastes modified with superabsorbent polymers." *Constr. Build. Mater.* 109 (Jan): 156–165. https://doi.org/10.1016/j.conbuildmat.2015.12.082.

Farzanian, K., B. Vafaei, and A. Ghahremaninezhad. 2019. "The behavior of superabsorbent polymers (SAPs) in cement mixtures with glass powders as supplementary cementitious materials." *Materials* 12 (21): 3597. https://doi.org/10.3390/ma12213597.

Farzanian, K., B. Vafaei, and A. Ghahremaninezhad. 2021. "The influence of the chemical composition of hydrogels on their behavior in cementitious materials." *Mater. Struct.* 54 (6): 244. https://doi.org/10.1617/s11527-021-01838-z.

Flores, J., M. Kamali, and A. Ghahremaninezhad. 2015. "Electrical resistivity measurement to study alkali-silica-reaction cracking in mortar." In *Proc., 7th Congress on Forensic Engineering, Forensic Engineering 2015: Performance of the Built Environment*. Reston, VA: ASCE. https://doi.org/10.1061/9780784479711.023.

Flores, J., M. Kamali, and A. Ghahremaninezhad. 2017. "An investigation into the properties and microstructure of cement mixtures modified with cellulose nanocrystal." *Materials* 10 (5): 498. https://doi.org/10.3390/ma10050498.

Gallagher, W. 1958. "FTIR analysis of protein structure." *Nature* 18: 662–666.

Ghosh, S. N., and S. K. Handoo. 1980. "Infrared and Raman spectral studies in cement and concrete (review)." *Cem. Concr. Res.* 10 (6): 771–782. https://doi.org/10.1016/0008-8846(80)90005-8.

Gollapudi, U. K., C. L. Knutson, S. S. Bang, and M. R. Islam. 1995. "A new method for controlling leaching through permeable channels." *Chemosphere* 30 (4): 695–705. https://doi.org/10.1016/0045-6535(94)00435-W.

Huang, H., G. Ye, and D. Damidot. 2013. "Characterization and quantification of self-healing behaviors of microcracks due to further hydration in cement paste." *Cem. Concr. Res.* 52 (Jun): 71–81. https://doi.org/10.1016/j.cemconres.2013.05.003.

Huang, H., G. Ye, C. Qian, and E. Schlangen. 2016. "Self-healing in cementitious materials: Materials, methods and service conditions." *Mater. Des.* 92 (Feb): 499–511. https://doi.org/10.1016/j.matdes.2015.12.091.

Hughes, T. L., C. M. Methven, T. G. J. Jones, S. E. Pelham, P. Fletcher, and C. Hall. 1995. "Determining cement composition by Fourier transform infrared spectroscopy." *Adv. Cem. Based Mater.* 2 (3): 91–104. https://doi.org/10.1016/1065-7355(94)00031-X.

Jain, J., and N. Neithalath. 2011. "Electrical impedance analysis based quantification of microstructural changes in concretes due to non-steady state chloride migration." *Mater. Chem. Phys.* 129 (1–2): 569–579. https://doi.org/10.1016/j.matchemphys.2011.04.057.

Jiang, Z., W. Li, and Z. Yuan. 2015. "Cement & concrete composites influence of mineral additives and environmental conditions on the self-healing capabilities of cementitious materials." *Cem. Concr. Compos.* 57 (Feb): 116–127. https://doi.org/10.1016/j.cemconcomp.2014.11.014.

Jonkers, H., and E. Schlangen. 2008. "Development of a bacteria-based self healing concrete." *Tailor Made Concr. Struct.* 109: 109. https://doi.org/10/dgt799.

Jonkers, H. M., and E. Schlangen. 2007. "Self-healing of cracked concrete: A bacterial approach." In *Proc., FRACOS6: Fracture Mechanics of Concrete and Concrete Structures*, 1821–1826. London: Taylor & Francis.

Jonkers, H. M., A. Thijssen, G. Muyzer, O. Copuroglu, and E. Schlangen. 2010. "Application of bacteria as self-healing agent for the development of sustainable concrete." *Ecol. Eng.* 36 (2): 230–235. https://doi.org/10.1016/j.ecoleng.2008.12.036.

Kamali, M., and A. Ghahremaninezhad. 2015. "Effect of glass powders on the mechanical and durability properties of cementitious materials." *Constr. Build. Mater.* 98 (Dec): 407–416. https://doi.org/10.1016/j.conbuildmat.2015.06.010.

Kamali, M., and A. Ghahremaninezhad. 2017. "An investigation into the influence of superabsorbent polymers on the properties of glass powder modified cement pastes." *Constr. Build. Mater.* 149 (Mar): 236–247. https://doi.org/10.1016/j.conbuildmat.2017.04.125.

Kamali, M., and A. Ghahremaninezhad. 2018a. "Effect of biomolecules on the nanostructure and nanomechanical property of calcium-silicate-hydrate." *Sci. Rep.* 8 (Sep): 1–16. https://doi.org/10.1038/s41598-018-27746-x.

Kamali, M., and A. Ghahremaninezhad. 2018b. "A study of calcium-silicate-hydrate/polymer nanocomposites fabricated using the layer-by-layer method." *Materials* 11 (4): 527. https://doi.org/10.3390/ma11040527.

Kang, S. H., S. G. Hong, and J. Moon. 2017. "Absorption kinetics of superabsorbent polymers (SAP) in various cement-based solutions." *Cem. Concr. Res.* 97 (Feb): 73–83. https://doi.org/10.1016/j.cemconres.2017.03.009.

Kang, S. H., S. G. Hong, and J. Moon. 2018. "Importance of monovalent ions on water retention capacity of superabsorbent polymer in cement based solutions." *Cem. Concr. Compos.* 88 (Jun): 64–72. https://doi.org/10.1016/j.cemconcomp.2018.01.015.

Khan, R. I., W. Ashraf, and J. Olek. 2021. "Amino acids as performance-controlling additives in carbonation-activated cementitious materials." *Cem. Concr. Res.* 147 (Jun): 106501. https://doi.org/10.1016/j.cemconres.2021.106501.

Khan, R. I., M. Intesarul, S. Siddique, E. N. Landis, and W. Ashraf. 2023. "Effects of amino acids on the multiscale properties of carbonated wollastonite composites." *Constr. Build. Mater.* 374 (Jul): 130816. https://doi.org/10.1016/j.conbuildmat.2023.130816.

Kua, H. W., S. Gupta, A. N. Aday, and W. V. Srubar. 2019. "Biochar-immobilized bacteria and superabsorbent polymers enable self-healing of fiber-reinforced concrete after multiple damage cycles." *Cem. Concr. Compos.* 100 (Feb): 35–52. https://doi.org/10.1016/j.cemconcomp.2019.03.017.

Lee, H., H. S. Wong, and N. R. Buenfeld. 2010. "Potential of superabsorbent polymer for self-sealing cracks in concrete." *Adv. Appl. Ceram.* 109 (5): 296–302. https://doi.org/10.1179/174367609X459559.

Lee, H. X. D., H. S. Wong, and N. R. Buenfeld. 2018. "Effect of alkalinity and calcium concentration of pore solution on the swelling and ionic exchange of superabsorbent polymers in cement paste." *Cem. Concr.*

Compos. 88 (Jun): 150–164. https://doi.org/10.1016/j.cemconcomp.2018.02.005.

Li, Q., Z. Liu, W. Chen, B. Yuan, X. Liu, and W. Chen. 2019. "A novel bio-inspired bone-mimic self-healing cement paste based on hydroxyapatite formation." *Cem. Concr. Compos.* 104 (Nov): 10335. https://doi.org/10.1016/j.cemconcomp.2019.103357.

Li, W., B. Dong, Z. Yang, J. Xu, Q. Chen, H. Li, F. Xing, and Z. Jiang. 2018. "Recent advances in intrinsic self-healing cementitious materials." *Adv. Mater.* 30 (17): 1705679. https://doi.org/10.1002/adma.201705679.

Liu, Q., Z. Chen, and Y. Yang. 2020. "Study of the air-entraining behavior based on the interactions between cement particles and selected cationic, anionic and nonionic surfactants." *Materials* 13 (16): 3514. https://doi.org/10.3390/ma13163514.

Lothenbach, B., G. Le Saout, M. Ben Haha, R. Figi, and E. Wieland. 2012. "Hydration of a low-alkali CEM III/B-SiO_2 cement (LAC)." *Cem. Concr. Res.* 42 (2): 410–423. https://doi.org/10.1016/j.cemconres.2011.11.008.

Magalhães, A. S. G., M. P. A. Neto, M. N. Bezerra, N. M. P. S. Ricardo, and J. P. A. Feitosa. 2012. "Application of FTIR in the determination of acrylate content in poly(sodium acrylate-CO-acrylamide) superabsorbent hydrogels." *Quim. Nova* 35 (7): 1464–1467. https://doi.org/10.1590/S0100-40422012000700030.

Martin, K., H. K. Tirkolaei, and E. Kavazanjian. 2021. "Enhancing the strength of granular material with a modified enzyme-induced carbonate precipitation (EICP) treatment solution." *Constr. Build. Mater.* 271 (Feb): 121529. https://doi.org/10.1016/j.conbuildmat.2020.121529.

Masoule, M. S. T., E. Baffoe, and A. Ghahremaninezhad. 2023. "On the physicochemical properties and foaming characteristics of proteins in cement environment." *Constr. Build. Mater.* 366 (Oct): 130204. https://doi.org/10.1016/j.conbuildmat.2022.130204.

Mechtcherine, V., and H.-W. Reinhardt. 2012. *Application of super absorbent polymers (SAP) in concrete construction*. New York: Springer.

Mignon, A., G. J. Graulus, D. Snoeck, J. Martins, N. De Belie, P. Dubruel, and S. Van Vlierberghe. 2014. "pH-sensitive superabsorbent polymers: A potential candidate material for self-healing concrete." *J. Mater. Sci.* 50 (2): 970–979. https://doi.org/10.1007/s10853-014-8657-6.

Mignon, A., D. Snoeck, P. Dubruel, S. Van Vlierberghe, and N. De Belie. 2017. "Crack mitigation in concrete: Superabsorbent polymers as key to success?" *Materials* 10 (3): 237. https://doi.org/10.3390/ma10030237.

Mignon, A., D. Snoeck, D. Schaubroeck, N. Luickx, P. Dubruel, S. Van Vlierberghe, N. De Belie, S. Van Vlierberghe, and N. De Belie. 2015. "PH-responsive superabsorbent polymers: A pathway to self-healing of mortar." *React. Funct. Polym.* 93 (Mar): 68–76. https://doi.org/10.1016/j.reactfunctpolym.2015.06.003.

Mollah, M. Y. A., W. Yu, R. Schennach, and D. L. Cocke. 2000a. "Fourier transform infrared spectroscopic investigation of the early hydration of Portland cement and the influence of sodium lignosulfonate." *Cem. Concr. Res.* 30 (2): 267–273. https://doi.org/10.1016/S0008-8846(99)00243-4.

Mollah, M. Y. A. A., W. J. Adams, R. Schennach, and D. L. Cocke. 2000b. "A review of cement–superplasticizer interactions and their models." *Adv. Cem. Res.* 12 (4): 153–161. https://doi.org/10.1680/adcr.2000.12.4.153.

Neithalath, N., J. Weiss, and J. Olek. 2006. "Characterizing enhanced porosity concrete using electrical impedance to predict acoustic and hydraulic performance." *Cem. Concr. Compos.* 36 (11): 2074–2085. https://doi.org/10.1016/j.cemconres.2006.09.001.

Pane, I., and W. Hansen. 2005. "Investigation of blended cement hydration by isothermal calorimetry and thermal analysis." *Cem. Concr. Res.* 35 (6): 1155–1164. https://doi.org/10.1016/j.cemconres.2004.10.027.

Prabahar, J., B. Vafaei, E. Baffoe, and A. Ghahremaninezhad. 2021. "The effect of biochar on the properties of alkali-activated slag pastes." *Constr. Mater.* 2 (1): 1–14. https://doi.org/10.3390/constrmater2010001.

Prabahar, J., B. Vafaei, and A. Ghahremaninezhad. 2022. "The effect of hydrogels with different chemical compositions on the behavior of alkali-activated slag pastes." *Gels* 8 (11): 731. https://doi.org/10.3390/gels8110731.

Raydan, N. D. V., L. Leroyer, B. Charrier, and E. Robles. 2021. "Recent advances on the development of protein-based adhesives for wood composite materials—A review." *Molecules* 26 (24): 7617. https://doi.org/10.3390/molecules26247617.

Reinhardt, H. W., and M. Jooss. 2003. "Permeability and self-healing of cracked concrete as a function of temperature and crack width." *Cem. Concr. Res.* 33 (7): 981–985. https://doi.org/10.1016/S0008-8846(02)01099-2.

Rodriguez-Navarro, C., C. Jimenez-Lopez, A. Rodriguez-Navarro, M. T. Gonzalez-Muñoz, and M. Rodriguez-Gallego. 2007. "Bacterially mediated mineralization of vaterite." *Geochim. Cosmochim. Acta* 71 (5): 1197–1213. https://doi.org/10.1016/j.gca.2006.11.031.

Rrustemi, T., Ö. G. Geyik, Z. Yüce, A. B. Özkaya, T. K. Öztürk, and A. Kilinç. 2020. "Acrylamide-encapsulated glucose oxidase inhibits breast cancer cell viability." *Turk. J. Biochem.* 45 (6): 811–816. https://doi.org/10.1515/tjb-2020-0247.

Schlangen, E., N. ter Heide, and K. van Breugel. 2006. "Crack healing age cracks in concrete." In *Measuring, monitoring and modeling concrete properties*, 273–284. Dordrecht, Netherlands: Springer. https://doi.org/10.1007/978-1-4020-5104-3_32.

Schröfl, C., V. Mechtcherine, and M. Gorges. 2012. "Relation between the molecular structure and the efficiency of superabsorbent polymers (SAP) as concrete admixture to mitigate autogenous shrinkage." *Cem. Concr. Res.* 42 (6): 865–873. https://doi.org/10.1016/j.cemconres.2012.03.011.

Shoulders, M. D., and R. T. Raines. 2009. "Collagen structure and stability." *Annu. Rev. Biochem.* 78 (1): 929–958. https://doi.org/10.1146/annurev.biochem.77.032207.120833.

Singh, M. 2007. "Structural interactions of globular proteins—Bovine serum albumin, egg albumin, and lysozyme, in aqueous medium, elucidated with molar volumes, viscosities, energy functions, and IR spectra from 293.15 to 303.15 K." *J. Appl. Polym. Sci.* 103 (3): 1420–1429. https://doi.org/10.1002/app.24626.

Smith, P. K., R. I. Krohn, G. T. Hermanson, A. K. Mallia, F. H. Gartner, M. D. Provenzano, E. K. Fujimoto, N. M. Goeke, B. J. Olson, and D. C. Klenk. 1985. "Measurement of protein using bicinchoninic acid." *Anal. Biochem.* 150 (1): 76–85. https://doi.org/10.1016/0003-2697(85)90442-7.

Snoeck, D., and N. De Belie. 2016. "Repeated autogenous healing in strain-hardening cementitious composites by using superabsorbent polymers." *J. Mater. Civ. Eng.* 28 (1): 04015086. https://doi.org/10.1061/(ASCE)MT.1943-5533.0001360.

Snoeck, D., L. Pel, and N. De Belie. 2020. "Autogenous healing in cementitious materials with superabsorbent polymers quantified by means of NMR." *Sci. Rep.* 10 (1): 1–6. https://doi.org/10.1038/s41598-020-57555-0.

Snoeck, D., D. Schaubroeck, P. Dubruel, N. De Belie, and N. De Belie. 2014a. "Effect of high amounts of superabsorbent polymers and additional water on the workability, microstructure and strength of mortars with a water-to-cement ratio of 0.50." *Constr. Build. Mater.* 72 (Feb): 148–157. https://doi.org/10.1016/j.conbuildmat.2014.09.012.

Snoeck, D., K. Van Tittelboom, S. Steuperaert, P. Dubruel, and N. De Belie. 2014b. "Self-healing cementitious materials by the combination of microfibres and superabsorbent polymers." *J. Intell. Mater. Syst. Struct.* 25 (1): 13–24. https://doi.org/10.1177/1045389X12438623.

Snoeck, D., L. F. Velasco, A. Mignon, S. Van Vlierberghe, P. Dubruel, P. Lodewyckx, and N. De Belie. 2015. "The effects of superabsorbent polymers on the microstructure of cementitious materials studied by means of sorption experiments." *Cem. Concr. Res.* 77 (Sep): 26–35. https://doi.org/10.1016/j.cemconres.2015.06.013.

Sondi, I., and E. Matijević. 2001. "Homogeneous precipitation of calcium carbonates by enzyme catalyzed reaction." *J. Colloid Interface Sci.* 238 (1): 208–214. https://doi.org/10.1006/jcis.2001.7516.

Tang, W., O. Kardani, and H. Cui. 2015. "Robust evaluation of self-healing efficiency in cementitious materials—A review." *Constr. Build. Mater.* 81 (Mar): 233–247. https://doi.org/10.1016/j.conbuildmat.2015.02.054.

Tantimongcolwat, T., C. Isarankura-Na-Ayudhya, A. Srisarin, H.J. Galla, and V. Prachayasittikul. 2014. "Polyacrylamide hydrogel encapsulated E. coli expressing metal-sensing green fluorescent protein as a potential tool for copper ion determination." *Excli J.* 13: 401–415.

Tourney, J., and B. T. Ngwenya. 2014. "The role of bacterial extracellular polymeric substances in geomicrobiology." *Chem. Geol.* 386 (Jan): 115–132. https://doi.org/10.1016/j.chemgeo.2014.08.011.

Ur Rehman, H., M. A. Nawaz, S. Pervez, M. Jamal, M. Attaullah, A. Aman, and S. A. Ul Qader. 2020. "Encapsulation of pectinase within polyacrylamide gel: Characterization of its catalytic properties for continuous industrial uses." *Heliyon* 6 (8): e04578. https://doi.org/10.1016/j.heliyon.2020.e04578.

Vafaei, B., K. Farzanian, and A. Ghahremaninezhad. 2020. "The influence of superabsorbent polymer on the properties of alkali-activated slag pastes." *Constr. Build. Mater.* 236 (Feb): 117525. https://doi.org/10.1016/j.conbuildmat.2019.117525.

Vafaei, B., K. Farzanian, and A. Ghahremaninezhad. 2021. "Effect of hydrogels containing nanosilica on the properties of cement pastes." *J. Compos. Sci.* 5 (4): 105. https://doi.org/10.3390/jcs5040105.

Valenzuela, C., L. Abugoch, C. Tapia, and A. Gamboa. 2013. "Effect of alkaline extraction on the structure of the protein of quinoa (*Chenopodium quinoa* Willd.) and its influence on film formation." *Int. J. Food Sci. Technol.* 48 (4): 843–849. https://doi.org/10.1111/ijfs.12035.

Vignaga, E., H. Haynes, and W. T. Sloan. 2012. "Quantifying the tensile strength of microbial mats grown over noncohesive sediments." *Biotechnol. Bioeng.* 109 (5): 1155–1164. https://doi.org/10.1002/bit.24401.

Wang, J. Y., D. Snoeck, S. Van Vlierberghe, W. Verstraete, and N. De Belie. 2014a. "Application of hydrogel encapsulated carbonate precipitating bacteria for approaching a realistic self-healing in concrete." *Constr. Build. Mater.* 68 (Jul): 110–119. https://doi.org/10.1016/j.conbuildmat.2014.06.018.

Wang, J. Y., H. Soens, W. Verstraete, N. De Belie, and N. De Belie. 2014b. "Self-healing concrete by use of microencapsulated bacterial spores." *Cem. Concr. Res.* 56 (Sep): 139–152. https://doi.org/10.1016/j.cemconres.2013.11.009.

Wehbe, Y., and A. Ghahremaninezhad. 2017. "Combined effect of shrinkage reducing admixtures (SRA) and superabsorbent polymers (SAP) on the autogenous shrinkage and properties of cementitious materials." *Constr. Build. Mater.* 138 (Oct): 151–162. https://doi.org/10.1016/j.conbuildmat.2016.12.206.

Weir, C. E., and E. R. Lippincott. 1961. "Infrared studies of aragonite, calcite, and vaterite type structures in the borates, carbonates, and nitrates." *J. Res. Natl. Bur. Stand. Sect. A Phys. Chem.* 65 (3): 173. https://doi.org/10.6028/jres.065A.021.

Wu, N., H. Pan, D. Qiu, and Y. Zhang. 2014. "Feasibility of EPS-producing bacterial inoculation to speed up the sand aggregation in the Gurbantunggut Desert, Northwestern China." *J. Basic Microbiol.* 54 (12): 1378–1386. https://doi.org/10.1002/jobm.201400355.

Xia, M. S., Z. T. Yao, L. Q. Ge, T. Chen, and H. Y. Li. 2015. "A potential bio-filler: The substitution effect of furfural modified clam shell for carbonate calcium in polypropylene." *J. Compos. Mater.* 49 (7): 807–816. https://doi.org/10.1177/0021998314525981.

Xu, J., and W. Yao. 2014. "Multiscale mechanical quantification of self-healing concrete incorporating non-ureolytic bacteria-based healing agent." *Cem. Concr. Res.* 64 (Nov): 1–10. https://doi.org/10.1016/j.cemconres.2014.06.003.

Yang, L., L. She, J. G. Zhou, Y. Cao, and X. M. Ma. 2006. "Interaction of lysozyme during calcium carbonate precipitation at supramolecular level." *Inorg. Chem. Commun.* 9 (2): 164–166. https://doi.org/10.1016/j.inoche.2005.05.026.

Ye, G., X. Liu, G. De Schutter, A. M. Poppe, and L. Taerwe. 2007. "Influence of limestone powder used as filler in SCC on hydration and microstructure of cement pastes." *Cem. Concr. Compos.* 29 (2): 94–102. https://doi.org/10.1016/j.cemconcomp.2006.09.003.

Ylmén, R., U. Jäglid, B. M. Steenari, and I. Panas. 2009. "Early hydration and setting of portland cement monitored by IR, SEM and Vicat techniques." *Cem. Concr. Res.* 39 (5): 433–439. https://doi.org/10.1016/j.cemconres.2009.01.017.

Yousuf, M., A. Mollah, T. R. Hess, Y. N. Tsai, D. L. Cocke, and A. Ftir. 1993. "An FTIR and XPS investigations of the effects of carbonation on the solidification/stabilization of cement based systems-portland type V with zinc." *Cem. Concr. Res.* 23 (4): 773–784. https://doi.org/10.1016/0008-8846(93)90031-4.

Zhu, B., Q. Li, W. Chen, W. Zou, and W. Chen. 2020. "A novel method of self-healing in cementitious materials by using polyacrylic hydrogel." *KSCE J. Civ. Eng.* 24 (11): 3406–3415. https://doi.org/10.1007/S12205-020-0090-6.

Zhu, Q., C. W. Barney, and K. A. Erk. 2015. "Effect of ionic crosslinking on the swelling and mechanical response of model superabsorbent polymer hydrogels for internally cured concrete." *Mater. Struct.* 48 (7): 2261–2276. https://doi.org/10.1617/s11527-014-0308-5.